Minor revisions

for "The Fate of a Southwest Pacific Bloom: Gauging the impact of submesoscale vs. mesoscale circulation on biological gradients in the subtropics"

by Alain de Verneil, Louise Rousselet, Andrea M. Doglioli, Anne A. Petrenko, and Thierry Moutin

In the following document we reproduce the .pdf files of our responses to the two anonymous reviewers, and append a marked-up version of the manuscript showing the changes made (removed sections in red, added in blue as done by latexdiff). The updated figures are also included (changes to Figs. 2, 3, 5, and 6), along with refined versions of the figures to be included in the Supplementary Material.

Response to Reviewer 1

for "The Fate of a Southwest Pacific Bloom: Gauging the impact of submesoscale vs. mesoscale circulation on biological gradients in the subtropics"

by Alain de Verneil, Louise Rousselet, Andrea M. Doglioli, Anne A. Petrenko, and Thierry Moutin

We thank Anonymous Reviewer 1 for their time and effort in formulating their review of the manuscript. Below we reproduce the reviewer's response and address their concerns along the way.

The topic of how primary production may be sustained by mesoscale and submesoscale circulations, particularly in the low nutrient subtropical gyres, is one of considerable broad interest. Yet it is an area where observations remain relatively few, particularly compared to modelling studies despite several of the latter indicating a major role for such physical processes. Motivated by encountering an unexpected phytoplankton bloom in such a region, the authors use a combination of in situ data and remote sensing to explore the potential role of the physical circulation. Their conclusion - that vertical nutrient flux from submesoscale processes is an unlikely control and that it is largely a 2D phenomenon with the mesoscale field advecting water against the mean flow - is one that seems best supported by the data. This is a very interesting result, particularly with the corollary that the mesoscale flow may be drawing iron away from the islands to trigger the bloom. However, there are a few aspects of the paper that I think need addressing before the manuscript can be published.

The paper essentially considers two possibilities: submesoscale vertical movement and mesoscale horizontal movement. The reader needs to have faith that both options have been thoroughly tested before the conclusion can be reached.

For the submesoscale, the largely horizontal structure of density and

discontinuities between surface and deep Chl are pretty convincing. I find the Richardson number argument less so given that the majority of submesoscale motions are confined in the surface boundary layer which is poorly sampled judging by Fig. 5. The authors should acknowledge this.

Response to Comment
Yes, indeed, the surface layer where one would expect most submesoscale motions is poorly sampled, since the mixed layer, according to our definition, averaged around 20 dBar for both the MVP and CTD datasets. Additionally, some data were cut off from this surface layer so that a direct comparison could be made to Ri using the ADCP data. The problems with the horizontal resolution of these features was mentioned in Sect. 2.4, Pg. 6, lines 26-29, as well as the Discussion. We have added the following changes (in bold) to the latter, where the possibility that the MVP survey did not fully resolve the features of interest is mentioned:

> Discussion, Sect. 4.2, Page 13, Line 24:
> If most submesoscale structures are expected to be in the mixed layer, which throughout this dataset was near 20 m, then the sub-kilometer R_D (here found to <200m) would not have been resolved by the MVP survey **since MVP horizontal resolution is $\sim$ 2 km. Besides problems of horizontal resolution, the shallow mixed layer also precluded complete vertical resolution by the underway MVP. As a result, though the summertime conditions present during the surveys lend support to reduced submesoscale circulation, the very same conditions make it difficult to state with confidence that the Ri and Ri_g methodology is entirely conclusive.** However, since the bloom of interest in these surveys spanned the top 40 m, and covered hundreds of kilometers in horizontal extent, these small features, should they have existed, would not have impacted the full depth range of the bloom, nor would they have significantly affected the horizontal advection of the entire bloom.

For clarity, Fig 5 should also have its colour scale changed so that

the blue-yellow transition is centred on zero - the value of interest.

Response to Comment

We have changed Fig 5 in accordance with this suggestion.

Additionally the MVP data being unfiltered will have internal waves (as acknowledged) which may misleadingly increase the lateral buoyancy gradient used for Ri_g. As an aside, might the striped nature of Fig 5 be due to internal waves?

Response to Comment

Regarding the aside, yes, the striped nature of Ri in Fig. 5 was most likely due to internal waves. In particular, near-inertial oscillations were observed during OUTPACE and are also likely a part of the ADCP data set during the MVP transects. Therefore, we looked into how filtering to remove these effects alters our results, which is summarized below.

The reviewer is astute in noting that by not horizontally filtering the density, an aliased internal wave may increase the horizontal buoyancy gradient, thus biasing Ri_g toward smaller values. For comparison, below is what Fig. 5 looks like when density is horizontally filtered, and we have also provided histograms of Ri_g's distribution for the unfiltered and filtered treatments over the top 50 m depth. Due to the homogeneity of density, the median decorrelation length scale (as judged by zero-crossings of the auto-correlation function) for density in the upper 50 m of T4 was approximately 34 km ($\sim$ 18 observations). Since this length scale is a significant fraction of the full-depth Rossby radius alluded to in the text (and in itself somewhat suggests the natural scale being mesoscale), below we present the 34 km filter (right panels) alongside a shorter 10 km filter treatment ($\sim$ 5 observations) for comparison (middle panels).

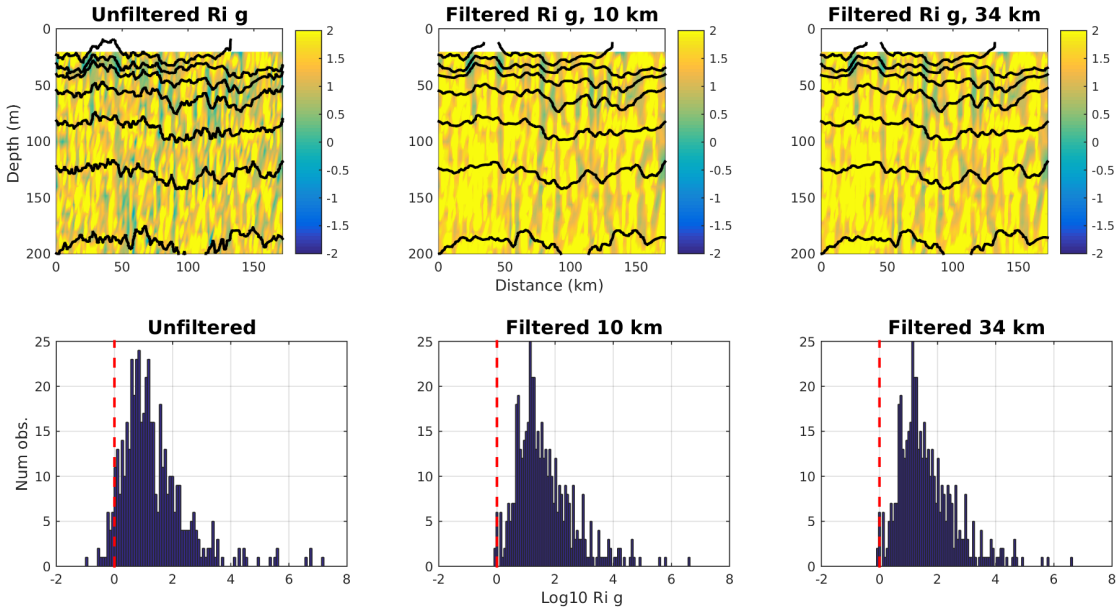

As one would expect, the filtered Ri_g has larger values (ie weaker vertical shear due to horizontal density structures), and only a few observations are at the value of 1 (0 in log-scale). The differences between the 10 km and 34 km filtering are virtually non-existent. For the purposes of this manuscript, since even with a biased signal the conclusion was that submesoscale shear was inconsequential, this further substantiates our claims. Therefore, we propose to keep the unfiltered Figure 5, but to add the above figure as part of the Supplementary material as Fig. S3 (Figures S1-S2 will concern the T-S figure requested). Additionally, we have added to the Materials and Methods section to refer to this sensitivity to filtering (changes in bold):

Materials and Methods, Sect. 2.2.2, Pg. 4, Line 30:
As discussed below (Sect. 2.4), the stratification was such that, even at 2 km resolution, density structures associated with balanced currents near the surface might be missed, so no additional filtering was applied to density in the MVP dataset despite possible aliasing of internal waves. **The Ri_g number analysis detailed in Sect. 2.4 can be sensitive to these aliased waves, and possibly bias the results. While, in general, this processing step should be considered, sensitivity analysis shown in the Supplementary Material (Fig. S3) revealed that the lack of filtering with the current dataset did not affect the resulting conclusions.**

For the mesoscale, the argument largely rests on advection using the altimetry derived flows and the Lyapunov exponents. Presumably if the sky was clear enough for such Chl images then SST is also available. This should also be shown in Fig. 6 (or in an equivalent new figure) as it gives greater faith in the analysis. SST does not have the complication of being a reactive tracer. i.e. does the SST field show the same/different matches with the FSLEs? Are they consistent with the hypothesis?

Response to Comment
As the reviewer has surmised, yes, SST data are available, and indeed SST is a more reliable tracer than Chl. Beyond the biological emphasis of this manuscript, Chl was used instead of SST because SST contained fewer visible gradients. We believe this is due to the fact that regional summertime heating at these latitudes is strong. The SST equivalent of Fig. 6 is provided below:

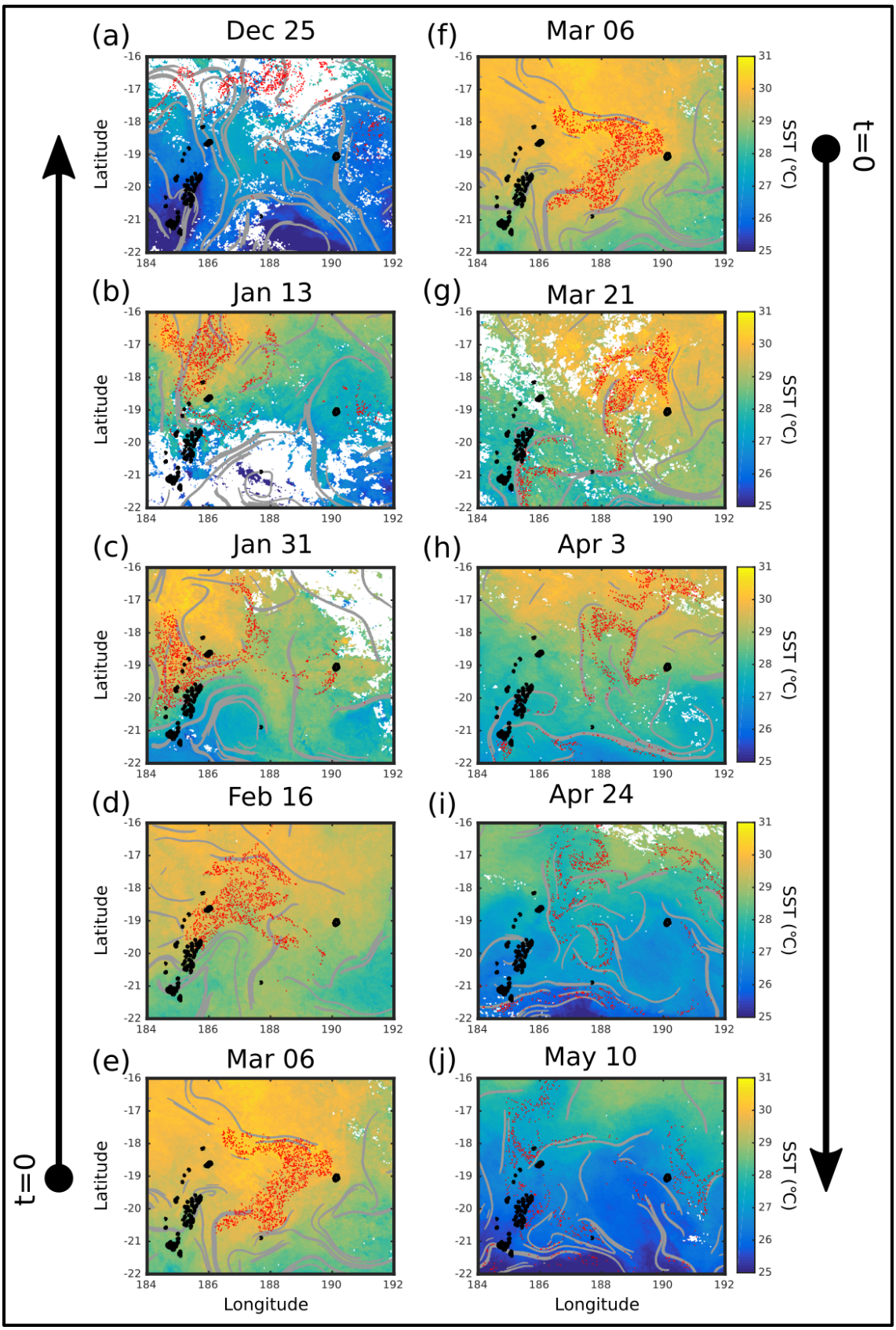
(a) Dec 25
(b) Jan 13
(c) Jan 31
(d) Feb 16
(e) Mar 06
(f) Mar 06
(g) Mar 21
(h) Apr 3
(i) Apr 24
(j) May 10
Latitude
Longitude
SST (°C)
t=0
t=0

The FSLEs that are the focus for the current manuscript (in areas of high chl-a) overlap regions of homogeneous SST. However, for certain dates FSLEs can be seen to correspond with SST fronts. Jan. 31, for example, indicates a recirculation of water south of the bloom's exit from the island region with cooler values to the South. Additionally, FSLEs and cooler water to the South are well-aligned in the last three panels (Apr 03 to May 10). Though the SST unfortunately does not contribute to the bloom's narrative, for completeness, we will add the above SST figure as supplementary material Fig. S4, and include the following references in both the Results and Discussion (changes in bold):

> Results, Sect. 3.4, Pg. 9, Lines 20-24:
> The remotely sensed distribution of surface chl-a, calculated FSLEs and ARIANE Lagrangian particle positions, over a period spanning 25 December, 2014 to 10 May, 2015 are shown in Fig. 6. FSLEs and particles are shaded gray and red, respectively, with 10% of the particles randomly selected for plotting in all subpanels. 25 December (Dec., all months hereafter shortened) was chosen as the starting point by visually examining the chl-*a* dataset for a pre-bloom period, with a bloom 'source' region identified on 13 Jan. centered at 186° E, 20° S. **The temporal evolution of FSLEs and the of Lagrangian particles superimposed on SST is reproduced in Fig. S4 of the Supplementary Material.**

> Discussion, Sect. 4.2, Pg. 14, Line 14:
> Evidently, chl-a is a reactive tracer and undergoes its own evolution, as shown by the shaded areas in Fig. 7b. **By contrast, the temporal evolution of SST, which does not suffer from this deficiency, did not display enough variability in the bloom region to confirm the efficiency of FSLEs or ARIANE particles in representing its advection (Fig. S4 in the supplementary material). This is most likely due to the strong, regional summertime heating that occurs at these latitudes.**

I find the particle tracking back to 25 December uncompelling, particularly given the very interesting idea in the Discussion of island iron being a factor. At first glance, the most striking feature of Fig 6 is a high chl patch on the east side of the island which seems about to be drawn away by the mesoscale flow. This is the basis of the authors' iron suggestion and they need to do it more justice. It would be interesting to see the results of seeding particles over the patch of high Chl next to the island on Jan 13 and running this forward to see how these waters correspond to those found later in the patch hosting LDB. If there are more satellite images available between Jan 13 and 31 in particular these should also be shown.

Response to Comment

We performed the requested Lagrangian analyses and below we provide the corresponding figures. First, Fig. 6 is re-created with a new particle initialization at the bloom's position near the island group on Jan 13 and advected in a forward time integration. Hereafter, we will refer to this as "Fig-6-Forward". Next, we provided the timeseries of Chl/FSLE/particle figures, starting from Jan 10 (a few days earlier than Jan 13) to Jan 31 with the Mar 06 particle seeding from the manuscript to fill in the gaps not presented in the original Fig. 6.

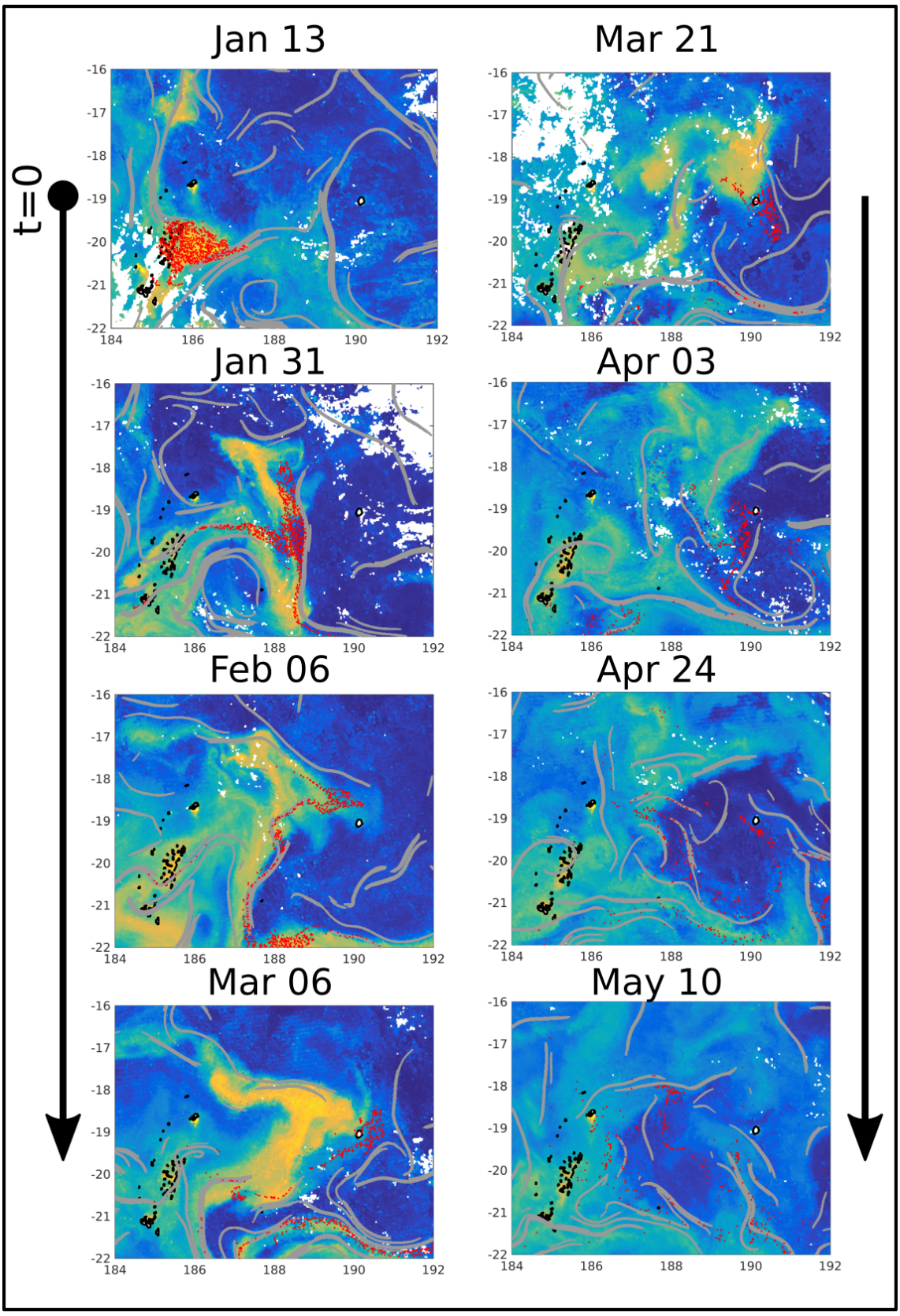
t=0
Jan 13
Mar 21
Jan 31
Apr 03
Feb 06
Apr 24
Mar 06
May 10
-16
-17
-18
-19
-20
-21
-22
184
186
188
190
192

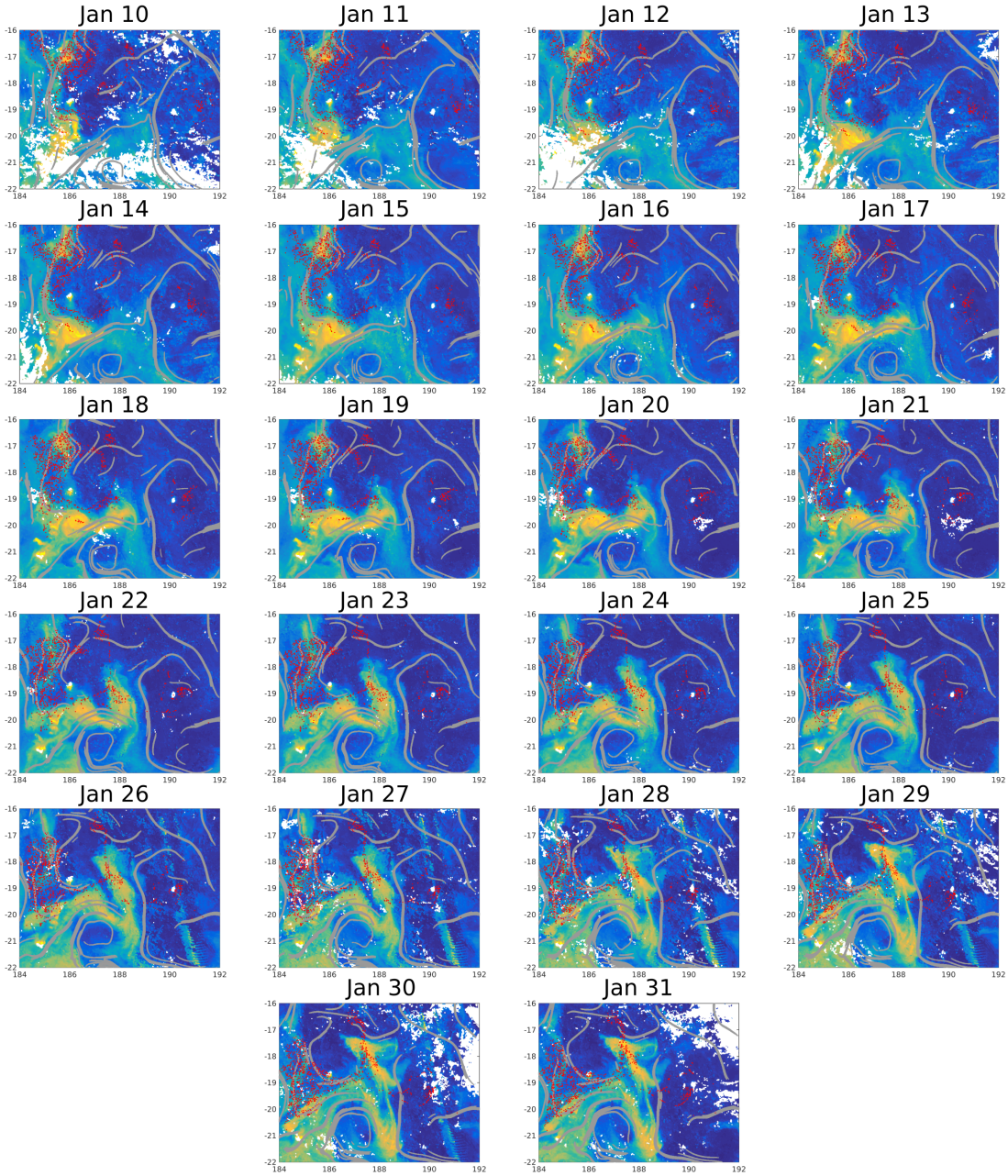

The additional Chl/FSLE/particle images between Jan 10 to Jan 31 document the bloom's exit from the island group in an eastward direction. The importance of the North-South FSLE barrier is evident during this period. The particles seeded in the bloom on Jan 13 (Fig-6-Forward) are largely absent from the bloom on Mar 06 (the seeding date in the original Fig. 6) and on Mar 21, the MVP sampling date. While disappointing for our argument, it is not surprising that chaotic particle trajecto-

ries are not strictly accurate two months after their initialization. This can be due to the reactive nature of chl-a, but also to the motions unresolved by our satellite data. The reactive nature of chl-a may be important, in particular for the blooms of this region that are sustained over long time periods by N_2 fixation. Symmetric to the lack of particles inside the bloom in Fig-6-Forward after two months, the backward integration shown in the original Fig. 6 produced few particles inside the bloom on Jan 13 near the island source region, also almost two months prior to seeding. If the errors result from unresolved physical motions, these results imply a temporal window beyond which particles have deviated from their "true course", and this is clearly less than two months. The particles in both scenarios, despite their limitations, both show eastward advection over time, which was one of the main results in our analysis. Additionally, while the particle positions are sensitive to the errors in the velocity field, the FSLE structures are relatively robust to these errors (mentioned in Sect. 2.4, Pg. 7, Line 7 with reference), and both particle seeding experiments show their role as flow barriers.

The original Fig. 6 was chosen to show the temporal evolution of the bloom both before its appearance on Jan 13 and after its decline starting in April. While the Dec 25 integration of particles may be uncompelling, the FSLEs are still relevant. Additionally, though there is much interest in following the bloom from its source and identifying its causes, one of the focuses of this work is in comparing which circulation regime creates biological gradients. In order to exemplify the ability of the mesoscale regime to form the gradients observed both by remote sensing and in situ data (e.g. MVP Transect 4), we feel the Mar 06 seeding is more relevant for the exposition of gradient formation (see original Fig. 6g). To prevent figure clutter but to also still show the results shown above, we propose adding both figures to the Supplementary Material as Figures S5 (Fig-6-Forward) and S6, respectively. We have modified the manuscript in the following ways:

Materials and Methods, Sec. 2.4, Pg. 7, Line 18 (additions in bold):
Lagrangian particles were spaced 1/50° ($\sim$ 2km) apart within the chl-a contour of 0.3 mg m^{-3}. **An additional forward particle experiment initialized on Jan 13, with a localization of the bloom near an island group, was also conducted, and these results are shown in supplementary material Fig. S5.**

Results, Sect. 3.4, Pg. 9, Lines 20-24 (previous changes repeated in italics, additions in bold):
The remotely sensed distribution of surface chl-a with a bloom 'source' region identified on 13 Jan. centered at 186° E, 20° S. *The temporal evolution of FSLEs and the Lagrangian particles superimposed on SST is reproduced in Fig. S3 of the Supplementary Material.* ***Additional chl-a data, between January 10 and 31, 2015, are also provided in Fig. S6.***

Discussion, Sect. 4.2, Pg. 14, Line 14 (previous changes repeated in italics, additions in bold, deletions with a strikethrough):
Evidently, chl-*a* is a reactive tracer and undergoes its own evolution, as shown by the shaded areas in Fig. 7b. *By contrast, the temporal evolution of SST, which does not suffer from this deficiency, did not display enough variability in the bloom region to confirm the efficiency of FSLEs or ARIANE particles in representing its advection (Fig. S3 in the supplementary material).* **Moreover, the particle positions are not reliable over long timescales. Few particles can be found in the bloom on Jan 13, when it was localized near a group of islands. Conversely, a second initialization experiment on Jan 13 failed to produce many particles in the bloom for Mar 06 and Mar 21 (Supplementary Material, Fig. S5). This limitation may be a result of chl-a being a reactive tracer or of unresolved motions in the altimetry-derived flow field. Therefore, while** the ability of the Lagrangian particles to ~~both~~ remain in the region of interest and to accurately represent elevated chl-a values (mostly above or near the 75th percentile) provides ~~strong~~ positive evidence that mesoscale flows were indeed advecting the bloom water **, after around two months the accumulated errors due to unresolved flows make direct inspection of particle position uninformative. The FSLEs, in comparison, do not suffer from this sensitivity.**

Discussion, Sect. 4.2, Pg. 14, Line 18-20 (additions in bold, deletions with a strikethrough):
Firstly, the ~~passage of particles~~ ***location of the bloom*** near an island group ***on Jan 13 (Fig. 6b, S5)*** ~~before and at the beginning of the bloom (Fig. 6A-b)~~ suggests a possible island effect in the ignition of the bloom. **Despite the fact the bloom's beginning was not captured by in situ data, we still suggest a mechanism responsible for causing the bloom.** Considering that N_2 fixation drove new production, and nearby stations SD12 and SD13 had detectable phosphate levels, alleviation of another necessary and limiting nutrient, iron, was possibly at work.

Discussion, Sect. 4.2, Pg. 14, Line 24-25 (additions in bold, deletions in strikethrough):
Secondly, the shifting FSLEs and **both** Lagrangian particle **experiments (Figs. 6, S5, and S6)** ~~tracks~~ demonstrate the general eastward advection of the bloom from its localized island source in Fig. 6b until its easternmost position in Fig. 6g.

On a more technical note the authors should discuss the consequences of using 30d integrations for FSLEs given the extent to which the 2d circulation is apparently changing in Fig. 6. How does the match up to tracers change if shorter integrations are used?

Response to Comment
The position of FSLEs, especially the strongest features, are fairly robust to the integration timescales. Long integration periods, in general, resolve smaller-scale features. Below we provide the FSLEs using 10, 15, 20, 25, and 30d integrations for Jan 31, when the bloom advected away from the island group and experienced strong North-South shear.

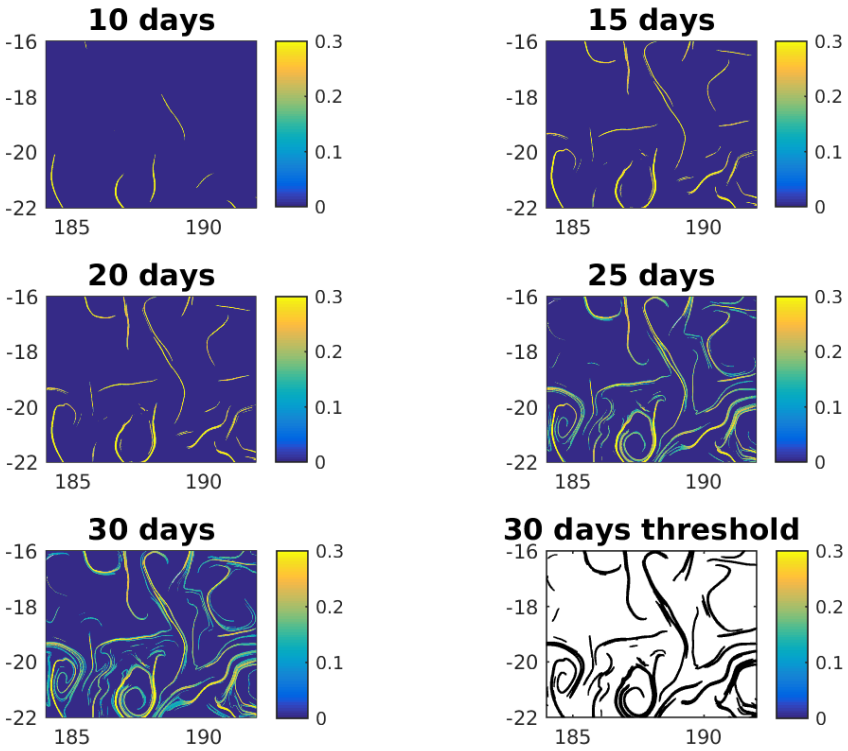

The largest change is between 20 and 25 days. Past this point, at 30 days, weaker structures appear, but are removed by the 0.15 d^{-1} threshold. Hence, in our case, there is no point in integrating with longer periods than 30 days, and the sensitivity of the FSLEs in our dataset should be minimal. We have added mentioned these sensitivity tests in the materials and methods:

Materials and Methods, Sec. 2.4, Pg. 7, Lines 6-7 (additions in bold):
The robustness of FSLE calculations to small-scale errors in velocity fields has been previously studied (Cotte et al., 2011). **The 30 day integration timescale we have chosen is likewise robust. Sensitivity analyses (not shown) indicate the strongest features are resolved with 10-15 day integrations, with finer detail emerging over 25-30 day integrations. The smallest structures are removed by a 0.15 day^{-1} threshold for the analysis in this study.**

I additionally have a number of more minor comments/suggestions:

- Given the issue with the salinities from the CTD I think there needs to be a T/S diagram using MVP data in Supplementary material to reassure the reader that density comparisons between Fig. 2 and 3 are reliable.

Response to Comment
We have plotted a T/S diagram of the MVP data for the calibration cast with SD13, shown below. Another CTD cast taken mid-way during other MVP sampling not presented in this manuscript is also shown. The first calibration casts were 3 km and 41 min apart, and the second set was 0.5 km and 53 min. apart.

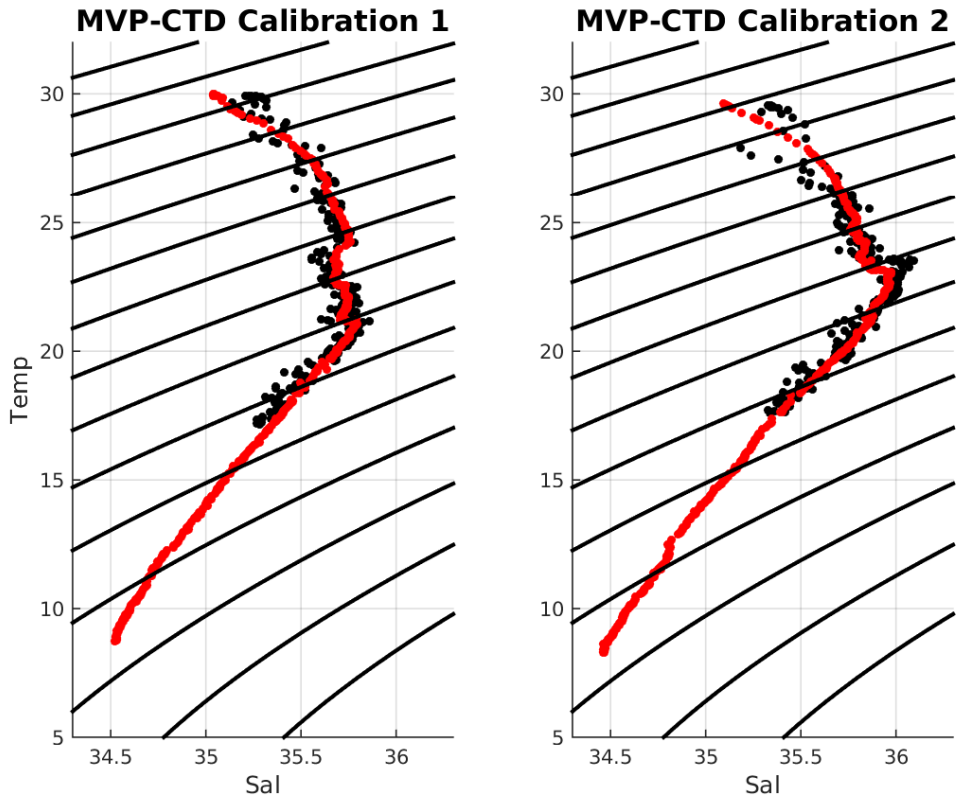

The variability in salinity is obvious, especially near the surface. This appears as a consequence of the fact that the sound speed is largely sensitive to temperature, and not salinity. As a result, the sound speed inversion to get salinity is relatively indeterminate. One would also expect variability to be greater at the surface, so this is not entirely surprising, but highlights that while the MVP allows for rapid surveying, this comes at the cost of increased signal variability vis a vis CTD rosette sampling. However, since the greater part of stratification was due to temperature, the variability due to salinity presents itself as small-scale salinity spikes in density that, while minimized in our post-processing, are still present (see density profiles below). The three profiles are off-set by 0.25 kg m^3 each.

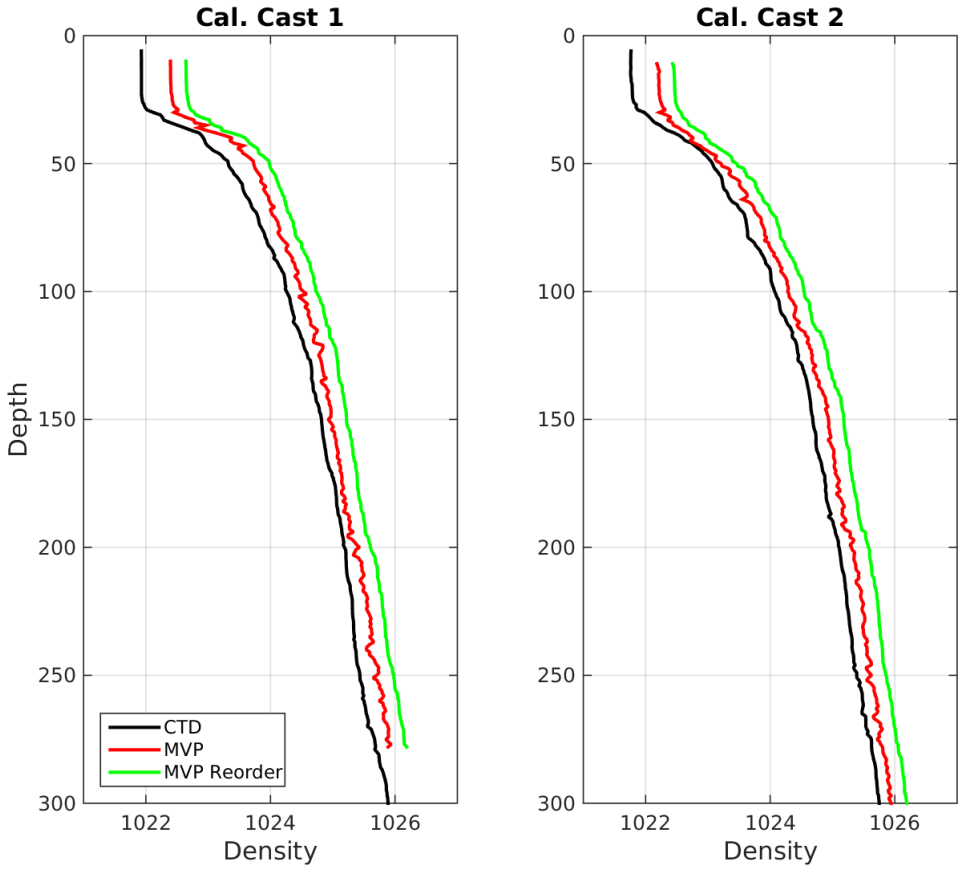

Once the density is re-ordered, the mis-fit between the calculated density of the MVP and the CTD is small enough (r^2 of 0.99) that the reader should be reassured of its utility for the plots and calculations. We propose to add the two above figures in the Supplementary material, and have made reference to them in the manuscript:

Materials and Methods, Sect. 2.2.2, Pg. 4, Lines 22-24 (additions in bold):
Due to technical difficulties onboard the ship, the conductivity sensor was swapped for a sound velocity sensor. In order to calculate salinity, the roots of the sound speed equation from Chen and Millero (1977) were matched with Mackenzie's linear approximation (1981). Sound speed and temperature data were lag-corrected to reduce salinity spiking. **The variability in calculated salinity from the soundspeed is larger than that calculated with conductivity (Fig. S1), but due to the greater contribution of temperature to stratification the resulting density profiles compare well with the CTD (Fig. S2, ρ =0.998, r^2 =0.996).**

- The location of the CTDs taken at LDB needs to be indicated on Fig. 2 and 6

Response to Comment
We have added the LDB CTD locations to both Fig. 2 and 6. However, due to the small spatial range of the CTD locations in relation to the area mapped, these locations all overlap and appear as one point.

- Fig. 3 looks like there might be an issue with quenching as the increase and decrease in surface Chl up to Mar 18 seem to have the expected daily cycle.

Response to Comment
The reviewer's observation of a daily cycle, most likely involving non-photochemical quenching, was noted by the authors as well. This effect would be problematic if the conclusions relied more sensitively upon the quantitative values of Chl observed. However, due to the large-scale change in surface Chl after Mar 18, the authors feel that the uncorrected contribution due to quenching does not impact the results. Nevertheless, to acknowledge the Reviewer's point, the quenching effect has been noted in the Materials and Methods, Results, and Discussion, as follows:

Materials and Methods, Sect. 2.2.1, Pg.3, Lines 26-27 (additions in bold):
Chl-*a* fluorescence was calibrated to chl-*a* extractions taken from the bottle samples throughout the cruise. **No corrections were made for the daily oscillations due to non-photochemical quenching.**

Results, Sect. 3.1.2, Pg. 8, Lines 12-13 (additions in bold):
From 18 March onward, the surface concentration of chl-*a* also decreased, whereas the chl-*a* max concentration increased and began to resemble a typical DCM distribution. ***Oscillations in the surface chl-a during the first half of the timeseries appear, likely due to non- photochemical quenching.***

Discussion, Sect. 4.1, Pg. 12, Line 17 (additions in bold):
Station LDB's CTD timeseries also showed the decrease of surface chl-*a* and the new formation of a DCM near 80 m. ***Fluctuations in the surface chl-a, a possible artifact of non-photochemical quenching, were small in relation to the large change in chl-a that occurs between the first and second halves of the timeseries.***

- This isn't really relevant to the main question behind the paper but why do the NO3 and PO4 profiles have a maximum around 120m?

Response to Comment
The maximum in nutrients in SD12 was noticed by the authors, as well. This local maximum in nitrate and phosphate is also reproduced in silicate. Additionally, a local oxygen minimum is also found at this depth. As a result, it is not likely a measurement error. Conversely, the temperature and salinity for SD12 don't show any discontinuities or anomalous trends. At depths greater than the 200m limit shown in Fig. 4, the usual trends of increasing nutrients are re-established for SD12. We interpret this local departure from a "classic" nutrient profile to be an intrusion at this depth of an another water mass, and without further data it is difficult to interpret its source. The water mass analysis of the entire OUTPACE

transect will be the scope of another paper from the special issue (Fumenia et al., this issue). As the reviewer notes, this does not directly impact the conclusions of the paper concerning the upper layer, but indeed it is not a mistake.

- If the hypothesis is of P controlling N fixation which drives the bloom it might be worth doing a scatter plot of PO4 versus Chl in surface waters (taking care with quenching) as a negative correlation would support this.

Response to Comment
The author's suggestion to test P control on N fixation, and thus growth, by plotting PO4 and Chl for a negative correlation is a good one. Unfortunately, the extremely low values of PO4 in the surface waters of LDB were below the measurement threshold, and so no reliable scatter plot can be made.

- There is no Section 2.3.1 first line, p.7

Response to Comment
Thank you for noting this, it has been corrected to just say Sect. 2.3 in the text.

- Figs 2 and 3 need the same colour scale

Response to Comment
Thank you again for seeing this, the change has been implemented.

Response to Reviewer 2

for "The Fate of a Southwest Pacific Bloom: Gauging the impact of submesoscale vs. mesoscale circulation on biological gradients in the subtropics"

by Alain de Verneil, Louise Rousselet, Andrea M. Doglioli, Anne A. Petrenko, and Thierry Moutin

We thank Anonymous Reviewer 2 for their time and effort in both reading the manuscript and writing their review. Below the review is reproduced with our responses to the concerns raised.

In this manuscript, the authors use hydrographic data as well as remotely sensed data to describe the evolution of a phytoplankton bloom which was observed during an oceanographic cruise. In-situ data used in this study comes from 3 stations, SD12, LDB and SD13, which were taken from Mar 11 thru Mar 21 2015. The authors conclude that the mesoscale eddy field is responsible for the horizontal advection of the bloom and do not find submesoscale motions to be relevant in the study region during that period, as diagnosed from the gradient and the balanced Richardson number.

The manuscript is well written and describes in detail the analysis and how the authors base their conclusions. At times, though, it reads much like a cruise report. I believe the authors could be more concise and to the point.

My main concern about the manuscript is what is exactly new in this study. The authors rule out the role of submesoscale motions in the horizontal distribution of the bloom. However, the main role of such motions in oligotrophic regions would be to ignite surface chlorophyll blooms by supplying limiting nutrients to the surface. This would occur, by definition, at the onset of the blooms. The in-situ sampling in the study took place from Mar 11 to Mar 25, when the bloom, as seen from the satellite images (Fig. 6) was relatively mature.

The authors point out that it probably started on the previous December in the vicinity of an island. They are probably correct that some

type of island-induced fertilization occurred, thus alleviating nutrient limitation (Dore et al. 2008), with chaotic advection transporting material over long distances, as shown previously (Rypina et al 2010). However, with the evidence shown it is not possible to infer if submesoscale processes were at work at the beginning of the bloom. Also, Law et al. 2011 report high rates of nitrogen fixation in an oligotrophic region after the passage of a tropical cyclone, which supposedly fertilized the ocean prior to a bloom. Strong winds may or may not be important for the ignition of the observed bloom, but the authors do not mention anything about it. The horizontal evolution of the bloom is most likely controlled by mesoscale currents, as shown in previous studies (Calil et al. 2011).

Response to Comment

In this section the reviewer first details the expected role of submesoscale vertical motion in starting a bloom, and that no in situ data in this study can corroborate submesoscale motion in the bloom's ignition. In the subsequent paragraph, the relative roles of island-induced fertilization, chaotic mesoscale advection, and strong wind forcing are mentioned with references to highlight the purported lack of novelty. Framed in this manner, we understand the reviewer's opinion and here we will better communicate the novelty in this work, and what hypotheses are being tested that contribute to the scientific literature.

Firstly, the reviewer is right in that the vertical motions due to submesoscale dynamics are probably of most interest to biologists, given their enhanced magnitudes relative to mesoscale motion (Mahadevan and Tandon, 2006). However, horizontal motions are also important for biological applications by influencing patch dynamics. Biological gradients are important because they can be hotspots of predation and other trophic interactions, where in terrestrial environments these are called 'edge effects' (Harris, 1988). Therefore, it matters which circulation regime is advecting a patch of bloom water. Both mesoscale and submesoscale regimes are expected to stir and strengthen gradients in a forward tracer variance cascade (Klein et al., 1998), but submesoscale motions would concentrate more of that variance at even smaller scales. Having more patches (and by definition more biological gradients at their boundaries) at small scales means greater opportunity

for these biological dynamics. Therefore, we have added the following to our introduction to better highlight this focus on horizontal motions and why it is important to diagnose submesoscale vs mesoscale regimes (and also remove unnecessary sentences mentioned later in the review):

> Introduction, Sect. 1, Page 2, Line 4 (additions in bold italics, deletions shown in strikethrough):
> Marine biological communities at any moment reflect a time-integration of the many complex interactions that occur both within the community and with the physical environment (Longhurst, 2010). ~~Despite the constant shifting and stirring that exist in a fluid medium, investigators often espouse the assumption that near "quiescent" gyres, the mean circulation's long timescale means that shipboard observations provide static, representative snapshots of a community that remains physically coherent long before and after in situ sampling. This assumption, however, is not always valid.~~ ***An important structuring mechanism of biological communities is the presence of gradients. In the terrestrial and conservation biology literature, these impacts are dubbed 'edge effects' (Harris, 1988), and have important implications for predation processes and species survival. Horizontal patch edges and biological transitions in the Ocean are liable to being advected by the surface circulation. Thus, it is necessary to identify the character of the flows that shape these horizontal gradients.***

We agree with the reviewer that it would be very interesting to know what happened at the beginning of the bloom. Nevertheless, as the reviewer noted, the proceeding of cruise events meant that we have no in situ data for the bloom at this period. Consequently, we focused on the "Fate" and not "Birth" of a Southwest Pacific bloom, as granted in the title of the paper. However, we do go into some detail regarding what can be inferred about the bloom's biogeochemical starting point in the Discussion. Therefore, as a means of better exploring the possible explanations for the bloom's origins, we have taken into account the mechanisms raised by the reviewer and tested whether these can be attributable to the bloom.

Since *Trichodesmium* blooms are rare (Westberry and Siegel 2006), they need to be treated on a phenomenological basis, as in the literature cited by the reviewer (Calil et al. 2011, Law et al. 2011). We thank the reviewer for pointing out these previous studies. Investigating these alternative mechanisms for the bloom in this manuscript can provide a further means of hypothesis testing on a rare event, which is a useful contribution to the scientific community.

Calil et al. (2011), cited by the reviewer, diagnosed upwelling motions due to mesoscale frontogenesis/frontolysis as estimated by the Omega equation (Hoskins et al., 1978), albeit with an alternate formulation and simplifying assumptions so that satellite altimetry data can be used. We have taken their approach, and used their Eqn. 2, ignoring the second deformation term, and calculated the right hand side of the equation, eg:

$$2f_0\frac{\partial}{\partial z}(\mathbf{v}_g \cdot \nabla_h \zeta_g)$$

simplified further to:

$$2f_0\mathbf{v}_g \cdot \nabla_h \zeta_g$$

Whether this quantity is negative or positive will imply a upwelling or downwelling velocity, respectively. Below is a figure of the currents, vorticity, and this Omega equation term for Jan 13, 2015, as the bloom is about the leave the island group. Each quantity is shown with its histogram directly below it (log_{10} of absolute magnitude for vorticity and Omega term).

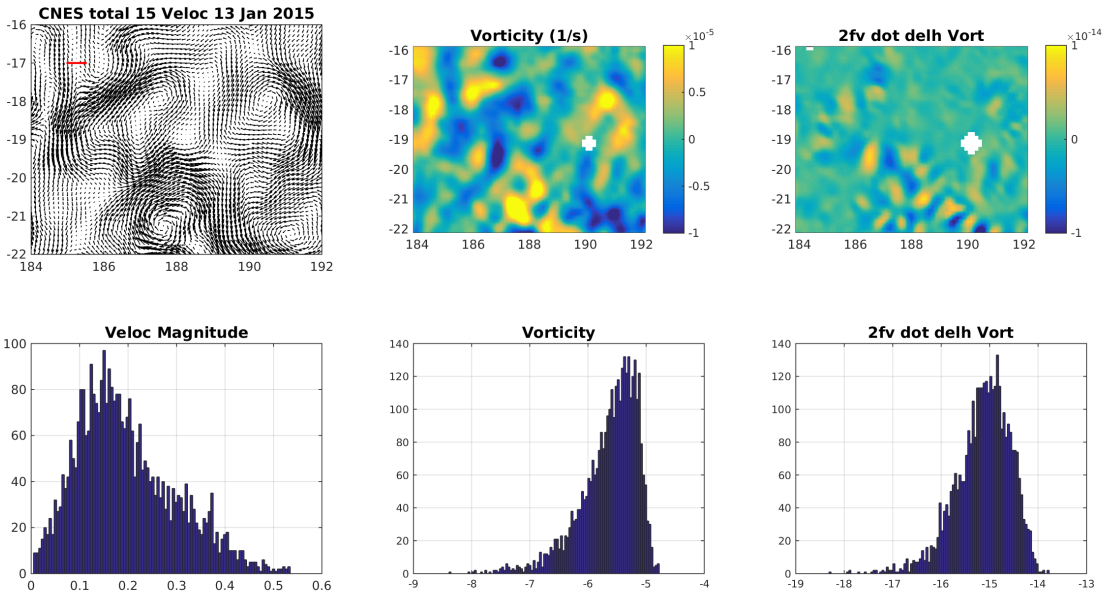

These distributions are similar for other days (figures and data can be provided, if requested). Of note, the omega equation upwelling/downwelling term has minima/maxima with O(10^{-14})s^{-3}, whereas in Calil et al. (2011), the values were three orders of magnitude higher. Additionally, the frontogenesis/frontolysis regions in Calil et al. (2011) coincided with low SST anomalies, which are not seen in our dataset (a SST version of Fig. 6 is to be added to the Supplementary Material in response to Reviewer 1).

Moreover, the upwelling cited in the 2008 bloom of Calil et al. (2011) advected nutrients from a 40 m deep mixed layer, where climatological data from station ALOHA indicate nutrient reservoirs exist. The in situ data from OUTPACE, with a shallower mixed layer near 20 m, show that phosphate, one of the limiting nutrients for nitrogen fixation, was not present immediately below this layer. Instead, the phosphocline was observed near 80 m depth for both LDB and SD12, the non-bloom station in the same region. High phosphate near the surface was instead only observed to the East, in SD13 associated with the subtropical gyre. The weak forcing, lack of SST gradients, and low phosphate in the upper 80 m help rule out this mechanism as judged by remote sensing data.

Calil et al. (2011) also highlight the requisite condition of 25°C for bloom ignition in the 2010 North Pacific bloom. The advancement of the 25° isotherm is invoked to explain the apparent eastward propagation of the large, contiguous bloom. Eastward mesoscale advection is discounted due to lack of evidence from

satellite altimetry data. For the OUTPACE bloom, the SST near the island group immediately before the bloom was mostly above 25°C, though small regions of water below 25°C can be found (see Jan 2015 subpanels of Chl below, with black dots for values $\leq$ 25°C). After Jan 10, however, only a very limited region is below this threshold, and yet only a subset of all the remaining warm water experienced a bloom.

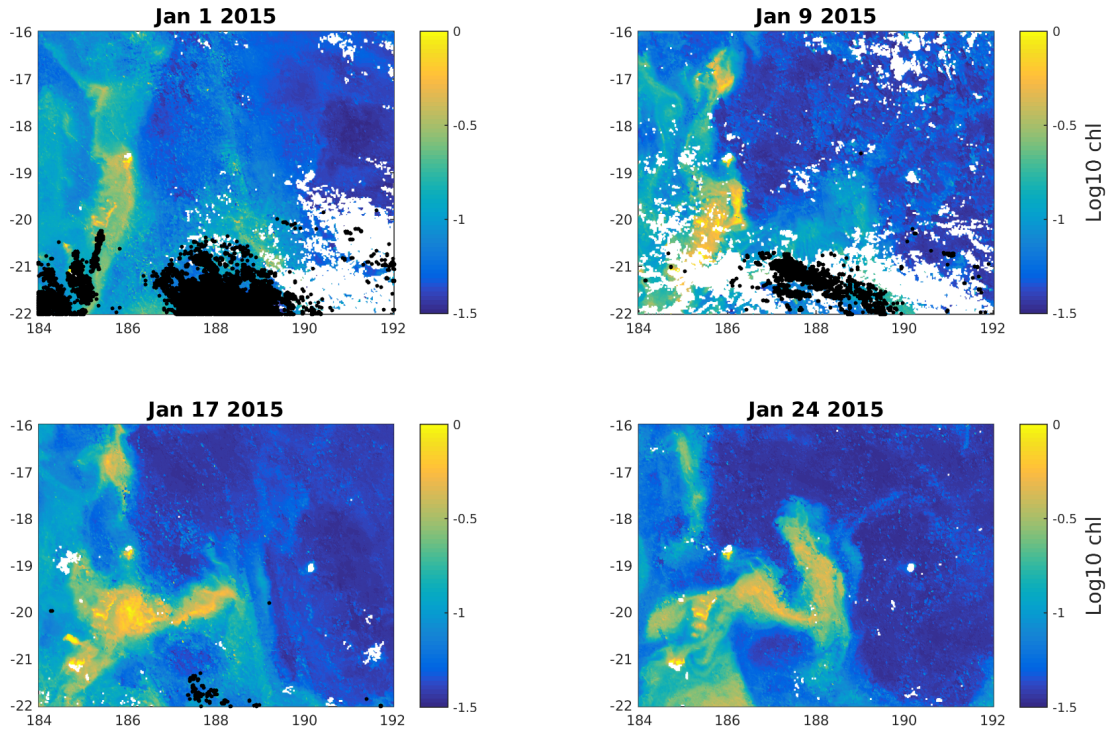

Therefore, while sufficiently warm waters may be ultimately better for diazotroph physiology (in particular *Trichodesmium*), our data support the notion that it is necessary but not sufficient to invoke a bloom. Calil et al. 2011 also noted this, with nutrients such as phosphate and iron being needed.

The reviewer points out the role of tropical cyclones in providing the necessary nutrients for blooms with reference to Law et al. (2011). Yes, wind forcing from strong events such as tropical cyclones can fertilize the ocean and bring about N_2 fixation blooms. The value-added altimetry products from CLS/CNES included an Ekman component, derived from the ECMWF ERA INTERIM windstress model. Below, moving left to right we plot the velocities without wind, with wind, and

the differences, respectively, for Jan 13. Immediately below these three panels are histograms of the u, v component and % magnitude ratio of the wind-nowind difference to the magnitude of the no-wind product.

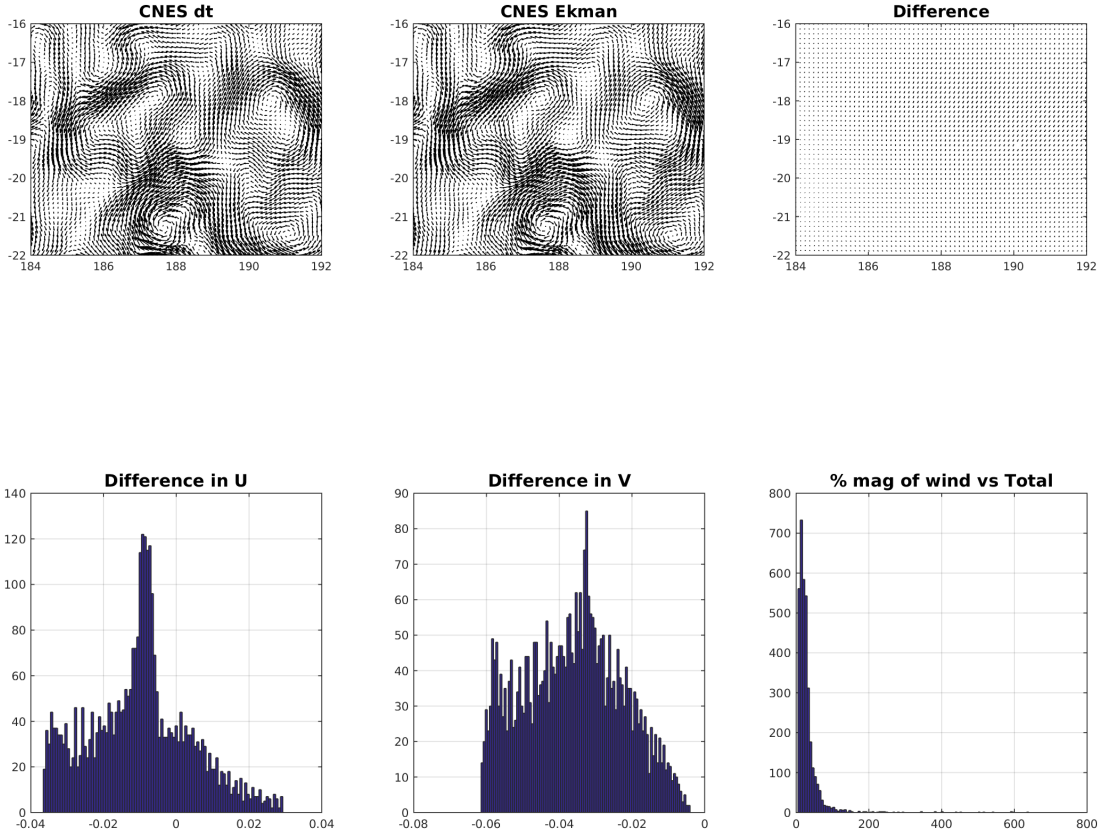

The differences between velocities with wind effects and without were small, and the magnitude differences in velocities averaged around 30% of the total. These results suggest little changes due to wind in the circulation. However, there was a strong wind forcing event within the OUTPACE region, just not near LDB. Cyclone Pam entered the Southwest Pacific in early March, and a drop in SST and increase in Chl followed in its wake. The relevant figures are shown below (the islands are the Vanuatu archipelago, top row is SST, bottom is Chl-a. Color scale is 25 to 31°C and -1.5 to 0 log_{10} Chl-a, respectively):

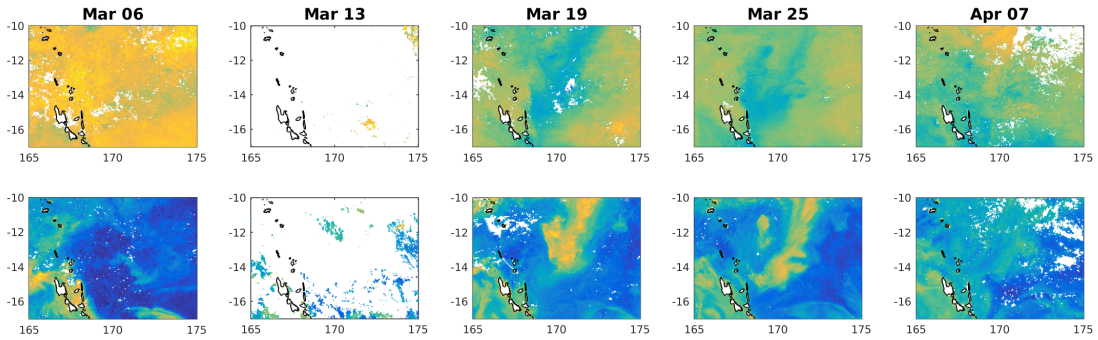

As can be clearly seen, the storm did indeed have a fertilizing effect. Unlike the LDB bloom, however, the elevated Chl signal did not last for an entire month. Therefore, in the face of an extreme forcing event, the biological response was transient in opposition to the LDB bloom, where there was no large-scale forcing and the bloom was persistent for over two months. While we cannot be certain that nitrogen fixation was a major factor in the storm-induced bloom, the longer timescale for the LDB bloom suggests that ongoing new production (we remind the reader that nitrogen fixation was directly observed in situ at LDB) was an important factor. This further validates our examination of the in situ data which, although not present for the bloom's ignition, can still be used to examine the circulation impacting the continuing new production being created.

In light of the previous examination of mechanisms elicited by our response to the reviewer's comments, we propose to amend our manuscript as follows:

The previous figures, which look at, in turn, frontogenetic/frontolytic forcing, SST thresholds, wind forcing, and a contemporaneous short-lived bloom due to wind forcing, will be added as Supplementary material. In particular, since in response to Reviewer 1 there are currently Figs. S1-6, these will constitute Figs. S7-10. Fig. S7 displays the frontogenetic forcing. Fig. S8 shows the wind-nowind differences. Fig. S9 has the timeseries of SST and Chl following Cyclone Pam. Finally, Fig. S10 shows the position of 25°C water.

The above discussion weighing alternative mechanisms for the bloom's ignition has been added in condensed form in the Discussion, starting where advective fluxes and forcing is considered:

Discussion, Sect. 4.1, Pg. 12, Line 1 (additions in bold):
These data therefore also remove the possibility of a massive diapycnal mixing event.
Similar surface blooms in oligotrophic regions have been investigated before, with varying mechanisms to explain their initiation. In particular, upwelling due to mesoscale frontogenesis and wind forcing, are possible causes for surface blooms (Calil et al., 2011, Law et al., 2011). While there are no in situ data during the bloom's appearance in mid-January 2015, sufficient data exist to judge these mechanisms, which would provide advective flux and diapycnal mixing, respectively. Upwelling due to mesoscale frontogenesis can be diagnosed using the Omega equation (Hoskins et al., 1978) with the assumptions employed by Calil et al. (2011) for its use with altimetry data. Calculating this forcing for the OUTPACE bloom resulted in values three orders of magnitude smaller than those for the 2008 bloom of Calil et al. (2011) (Fig. S7). As further comparison, climatological data from station ALOHA in that study place phosphate reservoirs for N_2 ***fixation at 40m depth, shallower than the depths observed during OUTPACE. These results, in addition with the lack of SST gradients one would expect (Fig. S4), make this mechanism unlikely.***

Another mechanism is strong wind forcing, such as that provided by tropical cyclones. These storms have been shown to fertilize blooms in oligotrophic waters (Law et al., 2011). Using the value-added altimetry dataset with wind component, the impact of wind was evaluated and found to be relatively small (Fig. S8) and could not create deep mixing. By contrast, another region in the OUTPACE domain witnessed the passage of Cyclone Pam in early March, 2015. The satellite imagery before and after its passage corroborate the fertilizing effect of storms in this region (Fig. S9). Whereas the LDB bloom lasted for over two months, this increase in chl-a lasted approximately a month. Therefore, given the lack of strong forcing, a mechanism must be invoked that can produce blooms of greater magnitude and duration than those produced by passing storms.

Passing reference to the temperature criterion will be added in the subsequent paragraph:

> Discussion, Sect. 4.1, Pg. 12, Line 4 (additions in bold italics):
> Diazotrophs, the organisms responsible for N_2 fixation, are normally concentrated in the surface layer ***in sufficiently warm water ($\geq$ 25°C in Calil et al., 2011).*** ~~, exactly where the bloom was found, and during station LDB~~ ***The LDB bloom was found in the upper surface layer, satellite SST was warmer than the 25°C threshold for its entirety (Fig. S10), and finally*** this process was observed directly (Caffin et al., this issue).

The authors claim to use a formulation from Thomas et al. 2013, based on the balanced Richardson number, to determine "how submesoscale the observed velocity shear is." However, the criteria described in Thomas et al. 2013, as seen by the pie chart in their Fig. 1, characterizes the flow as stable or unstable to a number of instabilities.

Moreover, it considers the relative vorticity of the flow field. Therefore, while I don't think submesoscale processes were at play during the survey, this diagnostic by itself is not fully accurate for the purposes intended in this study and may be misleading for readers.

Response to Comment

The reviewer is correct in noting that relative vorticity is included in the conditions described by Thomas et al., 2013 for different instabilities. To clarify, the function of Ri_g in our manuscript is not to primarily search for instabilities. Instability criteria were not the reason that the value of $Ri_g \leq 1$ was chosen to indicate the submesoscale regime. This choice instead comes from other studies (Mahadevan 2016, McWilliams 2016). Ri_g served as a convenient formulation isolating the balanced flow component contributed by submesoscale circulation.

True, relative vorticity is included in the treatment of Thomas et al. (2013), but this is mainly to give mention that inertial instability occurs when anticyclonic relative vorticity becomes stronger than planetary vorticity. Relative vorticity of one sign or another would not affect the value of Ri_g. Therefore, if the intention is to diagnose instability conditions, as the Reviewer suggests the relative vorticity needs to be taken into account. Additionally, the Ri_g diagnostic needs to be transformed into the ϕ_{Ri_b} variable presented in the pie charts of Fig. 1 in Thomas et al. (2013).

To make these distinctions clear, we have added the following to the Materials and Methods section:

> Materials and Methods, Sect. 2.4, Pg. 6, Line 7 (additions in bold, deletions in strikethrough):
> In submesoscale flows, instabilities such as Symmetric Instability (SI) appear when $Ri \leq 1$ (Stone, 1970). ~~In order to determine how "submesoscale" the observed velocity shear is,~~ ***The submesoscale regime is commonly accepted to begin near*** $Ri \sim$ ***1,*** $Ro \sim$ ***1 (Mahadevan 2016, McWilliams 2016). In order to diagnose dynamical regimes from in situ data,*** we used a formulation from Thomas et al. (2013) to find the geostrophic component of shear, expressed as:

Materials and Methods, Sect. 2.4, Pg. 6, Line 12 (changes in bold italics):
In this paper, we characterized the flow as submesoscale when Ri_g reached this value of 1.
The Ri_g diagnostic was originally designed for instability criteria. Here, we are not searching for instabilities. The fact that Ri_g solely looks at shear due to buoyancy gradients is useful for considering submesoscale features. In order to more fully investigate the instabilities that are possible in a given dataset, the relative vorticity is required in addition to Ri_g (see Fig. 1 in Thomas et al., 2013; for example, sufficient cyclonic vorticity can make a water column stable to SI below $Ri = 1$), which is out of the scope of this paper.

As a general comment, it has long been recognized that subtropical gyres, despite their low biomass, are far from being "oceanic deserts" (Emerson et al. 1997) as they are responsible for approximately half of the export of organic carbon of the oceans.

Response to Comment

We agree with the reviewer, that though subtropical gyres have low biomass, biological rates in the region are high and contribute to an appreciable fraction of organic carbon export. We have removed this characterization from the Introduction.

An additional comment: the authors tend to use sentences such as "investigators often espouse the assumption that" or "which are what most investigators focus on." These sentences, without specific references are vague and unfit for a scientific paper. The authors should explicitly cite the works or assumptions they are supposedly challenging or simply remove these sentences.

Response to Comment

The following sentences have been removed (in strikethrough):

Introduction, Sect. 1, Pg. 2, Lines 5-8 (Same deletion as shown in Pg. 3 of this document):
~~Despite the constant shifting and stirring that exist in a fluid medium, investigators often espouse the assumption that near "quiescent" gyres the mean circulation's long timescale means that shipboard observations provide static, representative snapshots of a community that remains physically coherent long before and after in situ sampling. This assumption, however, is not always valid.~~

Discussion, Sect. 4.2, Pg. 14, Lines 29-32:
This was possible due to the bloom occurring in water no associated with the coherent, elliptic structures that move west~~, and which are what most investigators focus on for mesoscale transport~~. Instead, the bloom occurred in water outside these structures, with tortuous trajectories hyperbolic in nature (Kirwan et al., 2003 **, Rypina et al., 2010**)

Additional References (not cited in original manuscript or Reviewer's submission)

Harris, L. D. (1988). Edge effects and conservation of biotic diversity. Conservation Biology, 2(4), 330-332.

Hoskins, B. J., Draghici, I., & Davies, H. C. (1978). A new look at the ωequation. Quarterly Journal of the Royal Meteorological Society, 104(439), 31-38.

Klein, P., Treguier, A. M., & Hua, B. L. (1998). Three-dimensional stirring of thermohaline fronts. Journal of marine research, 56(3), 589-612.

McWilliams, J. C. (2016, May). Submesoscale currents in the ocean. In Proc. R. Soc. A (Vol. 472, No. 2189, p. 20160117). The Royal Society.

Westberry, T. K., & Siegel, D. A. (2006). Spatial and temporal distribution of Trichodesmium blooms in the world's oceans. Global Biogeochemical Cycles, 20(4).

The Fate of a Southwest Pacific Bloom: Gauging the impact of submesoscale vs. mesoscale circulation on biological gradients in the subtropics

Alain de Verneil[1], Louise Rousselet[1], Andrea M. Doglioli[1], Anne A. Petrenko[1], and Thierry Moutin[1]

[1]Aix Marseille Univ, Université de Toulon, CNRS, IRD, Mediterranean Institute of Oceanography MIO, UM 110, 13288, Marseille, Cedex 09, France

Correspondence to: Alain de Verneil (alain.de-verneil@mio.osupytheas.fr)

Abstract. The temporal evolution of a surface chlorophyll-*a* bloom sampled in the Western Tropical South Pacific during the 2015 Oligotrophy to UlTra-oligotrophy PACific Experiment cruise is examined. This region is usually characterized by largely oligotrophic conditions, ie low concentrations of inorganic nutrients at the surface and deep chlorophyll-*a* maxima. Therefore, the presence of a surface bloom represents a significant perturbation from the mean ecological state. Combining in situ and remote sensing datasets, we characterize both the bloom's biogeochemical properties as well as the physical circulation responsible for structuring it. Biogeochemical observations of the bloom document the bloom itself, a subsequent decrease of surface chlorophyll-*a*, significantly reduced surface phosphate concentrations relative to subtropical gyre water farther east, and a physical decoupling of chlorophyll-*a* from a deep nitracline. All these characteristics are consistent with nitrogen fixation occurring within the bloom. The physical data suggest surface mesoscale circulation is the primary mechanism driving the bloom's advection, whereas balanced motions expected at submesoscales provide little contribution to observed flow. Together, the data provide a narrative where subtropical gyre water can produce significant chlorophyll-*a* concentrations at the surface that is stirred, deformed, and transported great distances by the mesoscale circulation. In this case, for the time period considered the transport is in an easterly direction, contrary to both the large-scale and mean mesoscale flow. As a result, future studies concerning surface production in the region need to take into account the role complex mesoscale structures play in redistributing subtropical gyre water.

1 Introduction

Subtropical gyres and their surroundings represent the largest surface biological provinces in areal extent. These regions are characterized by low standing stocks of phytoplankton biomass with deep chlorophyll-*a* (chl-*a*) maxima (DCM's) and low surface nutrient concentrations, and so have been dubbed the oligotrophic deserts of the sea. The South Pacific gyre (SPG) is the world's largest gyre and the most remote from large landmasses. Due to its remoteness, in situ data are generally lacking from the region; however, previous studies corroborate the oligotrophic status of this region (Claustre et al., 2008). Among oligotrophic areas, the SPG appears to be a low chlorophyll area with low N_2 fixation rates and high residual phosphate suggesting biological carbon pump inefficiency (Moutin et al., 2007). Flowing from the east, the waters from the SPG reach

the Western Tropical South Pacific (WTSP), which has been recently shown to be the world hotspot for N_2 fixation (Bonnet et al., in press), a process considered to be the largest external nitrogen source to the ocean (Sohm et al., 2011). Therefore, the physical processes that structure the gyre and nearby areas must be investigated.

Marine biological communities at any moment reflect a time-integration of the many complex interactions that occur both within the community and with the physical environment (Longhurst, 2010). ~~Despite the constant shifting and stirring that exist in a fluid medium, investigators often espouse the assumption that near "quiescent" gyres the mean circulation's long timescale means that shipboard observations provide static, representative snapshots of a community that remains physically coherent long before and after in situ sampling. This assumption, however, is not always valid.~~ An important structuring mechanisms of biological communities is the presence of gradients. In the terrestrial and conservation biology literature, these impacts are dubbed 'edge effects' (Harris, 1988), and have important implications for predation processes and species survival. Horizontal patch edges and biological transitions in the Ocean are liable to being advected by the surface circulation. Thus, it is necessary to identify the character of the flows that shape these horizontal gradients.

In recent decades, accumulating satellite data and high resolution modeling studies highlight how complex the surface ocean circulation really is beyond the mean flow, with several consequences. First, most kinetic energy in the surface ocean is found at the mesoscale, in eddies and frontal structures evolving over weeks and months (Stammer, 1997; Ferrari and Wunsch, 2009), so in a given field campaign these features can be the most important. Second, nonlinear eddy structures (ie 'rings') can be long-lived and transport water long distances (Chelton et al., 2007; Rousselet et al., 2016). These rings host their own biological dynamics, as well, which impact the biological pump (McGillicuddy et al., 2007; Nencioli et al., 2008; Moutin et al., 2012). Third, mesoscale motions can provide energy to the submesoscale through frontogenesis and filamentation, producing motions with much shorter timescales and relatively vigorous vertical circulation (Mahadevan and Tandon, 2006; Thomas et al., 2008; Mahadevan, 2016). Taken all together, these characteristics of surface ocean flow elucidate the importance of the mesoscale and submesoscale (hereafter (sub)-mesoscale when referred together) circulation in determining the spatial pattern of biological communities, with recent modeling work taking into account the role they play in moving around biological production at a regional scale (Nagai et al., 2015).

The WTSP presents an ideal laboratory in which to assess the impact of (sub)-mesoscale circulation upon planktonic communities in the gyre and nearby. In the WTSP, the SPG's northern limb, the South Equatorial Current (SEC), flows west into the Melanesian Archipelago group (MA) (Chaigneau and Pizarro, 2005). Though the SEC is relatively oligotrophic throughout, the depth of the DCM shoals as it moves west past these island groups, indicative of reduced oligotrophy. Sampling of this zonal gradient was the focus of the Oligotrophy to UlTra-oligotrophy PACific Experiment (OUTPACE) cruise during austral summer 2015 aboard the RV *L'Atalante* (Moutin and Bonnet, 2015). The main biogeochemical goals of OUTPACE concerned the study of biological production and its fate in a gradient of trophic conditions, from the ultra oligotrophic conditions of the SPG to the oligotrophic conditions of the MA (Moutin et al., this issue). During the cruise, however, a strong surface chl-*a* bloom was detected from satellite data and intensively sampled for five days during long duration station LDB. The presence of this surface bloom, itself a marked departure from the usual oligotrophic DCM pattern, in a region known to host production

fueled by N_2 fixation at the surface, brings into sharp focus the need to quantify and contextualize the relevant (sub)-mesocale circulation, also intensified near the surface, that might influence and structure this bloom.

In this study, we use a combination of in situ and remote sensing data to describe the bloom's distribution, evaluate its temporal evolution, and what role the (sub)-mesoscale current field may play in structuring it. We outline the sources of data, their processing, and the analyses required to investigate the bloom in Sect. 2. Subsequently, Sect. 3 summarizes the results from the calculations performed. After a discussion of the results in Sect. 4, we provide conclusions and possible applications of our approach in Sect. 5.

2 Materials and methods

2.1 Cruise sampling plan and context

In situ data for this study come from the OUTPACE cruise, conducted from 18 February to 3 April, 2015 in the WTSP on the French RV *L'Atalante*. Over a mostly zonal transect beginning west of New Caledonia and ending near Tahiti (Fig. 1), the ship sampled in two main ways: first, the short duration (SD) stations, and second the long duration (LD) stations. For the 15 SD stations, referred to by their number in chronological order, conductivity-temperature-depth (CTD) casts and biogeochemical measurements were taken over a 24 h period, as described in (Moutin et al., this issue). During the three LD stations, referred to as stations LDA, LDB, and LDC, a quasi-Lagrangian drift array was deployed with sediment traps. The ship largely followed the trajectory of this array. Multiple CTD casts were performed, spaced every 3 h. The position of each station was chosen using the SPASSO software suite (Doglioli, 2013), which analyzes near real-time remote sensing data so that an onshore collaborator can provide daily updates regarding the location of possible coherent structures such as eddies (Doglioli et al., 2013). Station LDB was selected because of the large surface chl-*a* signal as seen from satellites (Fig. 1b). The data used specifically in this study derived from SD12, LDB, and SD13. For these purposes, we defined the general region of interest as 184° E to 192° E and 22° S to 16° S (Fig. 1b).

In situ sampling for SD12, LDB, and SD13 took place during 11-12, 14-20, and 21 March, 2015, respectively. Before the deployment of the drift array during LDB, a survey of the area was conducted by a Moving Vessel Profiler (MVP; Brooke Oceanographic) platform, allowing for high-resolution CTD profiles over three separate transects (T1,T2, and T3 in Fig. 2a). Subsequent to the multi-day drift array experiments, a final MVP transect was conducted, as well (T4).

2.2 In situ data

2.2.1 CTD, bottle data, MLD and nitracline depth

The shipboard CTD rosette was deployed four times at SD12, 47 times during LDB, and once for SD13. The rosette layout was the Seabird SBE 9+ CTD-rosette (CR), with two CTDs installed on the rosette and a chl-*a* fluorometer (Chelsea Aqua 3). CTD data were calibrated and processed post-cruise using Sea-Bird Electronics software into 1 m bins. Chl-*a* fluorescence

was calibrated to chl-*a* extractions taken from bottle samples throughout the cruise. No corrections were made for the daily oscillations due to non-photochemical quenching.

Subsequent to CTD processing and calibration, each profile's density was reordered to be stable so that small, residual overturns were removed. Casts were spaced approximately 3 h apart, so density and chl-*a* were interpolated to a regular 3 h interval using cubic polynomials. A horizontal smoothing of density was performed using a 'lowess' filter with a window of four datapoints, equivalent to 12 h. This time span, designed to remove some internal waves, is $\sim \frac{1}{3}$ of the inertial period ($\sim$ 36 h), and does not remove the movements present due to near-inertial oscillations, a dominant signature in the shipboard acoustic doppler current profiler (SADCP) data (Bouruet-Aubertot et al., this issue).

Mixed layer depth (MLD) was calculated using a threshold density deviation of 0.03 $\mathrm{kg\ m^{-3}}$ from the value at a reference depth. The CTD profiles post-calibration did not always contain surface values, so a 10 m reference depth was used, similar to de Boyer Montégut et al. (2004).

Measurements of dissolved nitrate and phosphate concentrations were conducted for two casts at SD12, seven casts at LDB, and the single cast of SD13. The nitrate and phosphate concentrations were measured using continuous flow analysis (SEAL AutoAnalyzer 3) following the procedures in Aminot and Kérouel (2007). Quantification limits for all nutrients are 0.05 $\mu\mathrm{mol\ kg^{-1}}$. LDB nitracline depth was calculated for the last CTD associated with the drift-array recovery. The nitracline depth (D_{NO_3}) and its slope (S_{NO_3}) were calculated performing a linear fit with the first three measurements above the threshold of 0.05 $\mu\mathrm{mol\ kg^{-1}}$, resulting in D_{NO_3} = 121m and S_{NO_3} = 48 $\mu\mathrm{mol\ m^{-4}}$. The density anomaly at D_{NO_3} for this cast, 24.34 $\mathrm{kg\ m^{-3}}$, was subsequently used for the rest of the LDB time series.

2.2.2 MVP

The MVP was used during four transects, three (T1-T3) before LDB and one after (T4) (Fig. 2a). Prior to LDB, we have: T1, going Northwest to Southeast; T2, going South to North; and T3, North to South in the same path as T2. For these three transects, a total of 388 casts spanning $\sim$700 km distance were obtained, producing an average horizontal resolution of $\sim$2 km. Subsequent to LDB, T4 traveled west to east from LDB's position, resulting in 95 casts over $\sim$170 km horizontal distance.

The MVP vehicle sampled vertically by freewheeling the synthetic cable attached to the MVP fish, allowing for a near-vertical descent at $\sim$4 $\mathrm{m\ s^{-1}}$. At a prescribed depth (here, 350 dBar), the brake was applied to the computer-controlled winch and the fish automatically brought back to the surface. Only down-casts were used in this dataset due to the deployment method.

Onboard the fish was a rapid response AML Micro conductivity sensor, thermistor, and Wetlabs Wetstar chl-*a* fluorometer. Due to technical difficulties onboard the ship, the conductivity sensor was swapped for a sound velocity sensor. In order to calculate salinity, the roots of the sound speed equation from Chen and Millero (1977) were matched with Mackenzie's linear approximation (1981). Sound speed and temperature data were lag-corrected to reduce salinity spiking. The variability in calculated salinity from the soundspeed is larger than that calculated with conductivity (Fig. S1), but due to the greater contribution of temperature to stratification the resulting density profiles compare well wtih the CTD (Fig. S2, $\rho = 0.998$, $r^2 = 0.996$).A previous study utilizing MVP data found an operational threshold binning of $\sim$1m in the vertical (Li et al., 2012), which we followed here. Temperature and calculated salinity were calibrated to the station SD13 CTD cast made

adjacent to and soon after the last MVP profile of T4. Chl-*a* values were calculated by calibrating to the already calibrated CTD fluorometer values for SD13, as well.

MVP density profiles, as with CTD data, were first reordered to be statically stable. In contrast to the CTD data, horizontal distance, and not time, is the relevant variable. As discussed below (Sect. 2.4), the stratification was such that, even at 2 km resolution, density structures associated with balanced currents near the surface might be missed, so no additional filtering was applied to density in the MVP dataset despite possible aliasing of internal waves. The Ri_g number analysis detailed in Sect. 2.4 can be sensitive to these aliased waves, and possibly bias the results. While, in general, this processing step should be considered, sensitivity analysis shown in the Supplementary Material (Fig. S3) revealed that the lack of filtering with the current dataset did not affect the resulting conclusions.

In order to determine when the ship was in the surface bloom, a threshold value was chosen. Inspection of chl-*a* in the upper 20 m revealed a bi-modal distribution. As a result, the value of 0.13 $\mu\mathrm{g\ L^{-1}}$, well above the lower mode and representing the 66% value of the cumulative distribution function, was selected. Therefore, by our definition the MVP entered the surface bloom when the average value of chl-*a* in the top 20 m surpassed this value. Additionally, the MLD for the MVP transects were calculated from the same method as the CTD casts, by finding the depth where density surpasses 0.03 $\mathrm{kg\ m^{-3}}$ above the value at 10 m.

2.2.3 SADCP

The RV *L'Atalante* has two SADCPs, RDI Ocean Surveyors with frequencies of 75 kHz and 150 kHz. In order to maximize vertical resolution, we use the 150 kHz data in this study. Single ping data were collected into 2 min intervals, with vertical bins spanning 8 m. Binned data were processed with the Cascade (Le Bot et al., 2011) software package provided by IFREMER. The Cascade procedure corrects for, among other quantities, the horizontal SADCP/navigation misalignment as well as misalignment of the horizontal plane due to ship roll. In addition, within Cascade the barotropic tidal component was removed using the TOPEX/POSEIDON inverse model (Egbert et al., 1994).

2.3 Remote sensing data

Satellite-derived data (eg u,v, sea surface height, and surface chl-*a*) from altimetry and ocean color data were produced specifically for OUTPACE in the WTSP by Ssalto/Duacs and CLS with support from CNES. The procedures used to generate the data are similar to those described in (d'Ovidio et al., 2015), with the result that these products provide higher resolution and quality control measures than is typically available from global products. As described in the following paragraphs, some of these products were produced post-cruise in delayed-time, while others were provided during the cruise in near real-time.

Maps of altimetry were generated delayed-time by merging along-track observations from the Jason-2, Saral-AltiKa, Cryosat-2, and HY-2A missions. The regional OUTPACE domain spans 140° E to 220° E, and 30° S to the equator, over the yearlong period of June 2014 to May 2015. The regional product has a resolution of $\frac{1}{8}^\circ$ using the FES2014 tidal model, and the CNES_CLS_2015 mean sea surface. In order to produce this increase in resolution, among other measures region-specific noise measurements and correlation scales were calculated. Beyond the determination of merged absolute dynamic topography

and its currents, corrections for cyclogeostrophy and Ekman effects at both the surface and 15 m depth have been included in separate products. Comparisons between Surface Velocity Program drifters deployed during OUTPACE and numerical Lagrangian particle experiments using these different products indicated that inclusion of an Ekman velocity component at 15 m produced a more accurate trajectory (Rousselet et al., this issue). Therefore, the Ekman-inclusive altimetry product was used in the present study.

Both sea surface temperature (SST) and surface chl-*a* composite maps were also generated by CLS/CNES. These products were generated in near real-time during the OUTPACE campaign. Each map, with a $\frac{1}{50}^{\circ}$ resolution, uses a 5 day weighted mean of Suomi/NPP/Viirs measurements. The dataset spans from December 2014 to early May 2015.

2.4 Dynamic diagnostics and tools

The determination of the dynamical character of in situ currents surrounding the LDB bloom was implemented with use of the Richardson (Ri) number parameter. Classically, the gradient Ri number is defined as:

$$Ri = \frac{N^2}{\left(\frac{\partial \boldsymbol{u}}{\partial z}\right)^2} \tag{1}$$

with N^2, the stratification, being the square of the Brunt-Väisälä frequency, and $\frac{\partial \boldsymbol{u}}{\partial z}$ being the vertical shear of horizontal velocity. Ri is useful in characterizing differing regimes of flow, for example, the classical $Ri < \frac{1}{4}$ Kelvin-Helmholtz condition for instability. In submesoscale flows, instabilities such as Symmetric Instability (SI) appear when $Ri \leq 1$ (Stone, 1970). The submesoscale regime is commonly accepted to being near $Ri \sim 1$, $Ro \sim 1$ (Mahadevan, 2016; McWilliams, 2016).In order to ~~determine how "submesoscale" the observed velocity shear is~~diagnose dynamical regimes from in situ data, we used a formulation from Thomas et al. (2013) to find the geostrophic component of shear, expressed as:

$$Ri_g = \frac{f^2 N^2}{|\nabla_h b|^2} \tag{2}$$

where $b = -\frac{g\rho}{\rho_0}$ is the buoyancy (with g the gravitational constant, ρ the density, and ρ_0 a reference density), f is the Coriolis parameter, and ∇_h is the horizontal components of the gradient operator. In this paper, we characterized the flow as submesoscale when Ri_g reached this value of 1.

The Ri_g diagnostic was originally designed for instability criteria. Here, we are not searching for instabilities. The fact that Ri_g solely looks at shear due to buoyancy gradients is useful for considering submesoscale features. In order to more fully investigate the instabilities that are possible in a given dataset, the relative vorticity is required in addition to Ri_g (see Fig. 1 in Thomas et al., 2013; for example, sufficient cyclonic vorticity can make a water column stable to SI below $Ri = 1$), which is out of the scope of this paper.

The determination of Ri required combining the MVP data for the numerator and SADCP data for the denominator, and so is limited in resolution by the SADCP bins. Therefore, in calculating N^2, 8 m bins were produced by averaging the central finite differences from the 1 m density profile. Since we wished to characterize submesoscale phenomena, the horizontal gradient required for Eq.2 was left as is, without further re-binning. The calculation of Ri_g was also calculated at the same 8 m resolution.

By assuming balanced flow, we can estimate the horizontal scale of density structures in a layer with the first internal Rossby radius of deformation, approximated by Pedlosky (2013) as:

$$R_D = \frac{NH}{\pi f} \tag{3}$$

where H is the depth of the water column (for non-constant stratification, this becomes an integral over depth). As a result, apart from latitude and depth, stratification plays a major role in determining at which horizontal scales one would expect to see balanced motions. Typically, the entire water column is used in this calculation, though, for order-of-magnitude approximations, other depths may be used. For example, a 5000 m CTD cast near station LDC during OUTPACE (not shown) provided a radius of 65.2 km, consistent with a global climatological atlas for this region (Chelton et al., 1998). The average stratification during LDB produced scales of 160 m, 570 m, 2.7 km, 5.8 km, and 9.7 km for the top 20, 30, 50, 100, and 200 m, respectively. Using these scales, the horizontal resolution of the MVP transects sufficiently resolved features affecting layers comprising the upper 50 m and deeper.

The mesoscale structuring of the chl-*a* bloom was evaluated based on altimetry-derived finite size Lyapunov exponents (FSLE), computed following the algorithm of d'Ovidio et al. (2004). FSLEs were calculated by time-integrating trajectories on a grid using the velocities described in Sect. 2.3~~.1~~. The trajectories were found with a fourth-order Runge-Kutta method with a 6 h timestep. Particles were initially separated by 0.05° (the grid resolution) and reached a final separation of 0.6°. Velocity fields were linearly interpolated in space and time.

All FSLEs were calculated using 30 day backward integrations, meaning that the 'final' separation reflects initial displacements that were subsequently brought together (ie convergence). FSLE maximal values often form lines, or ridges, that were used to identify possible frontal zones of enhanced strain, along which tracer gradients should generally align. The robustness of FSLE calculations to small-scale errors in velocity fields has been previously studied (Cotté et al., 2011). The 30 day integration timescale we have chosen is likewise robust. Sensitivity analyses (not shown) indicate the strongest features are resolved with 10-15 day integrations, with finer detail emerging over 25-30 day integrations. The smallest features are removed by a 0.15 day^{-1} threshold for the analysis in this study. Additionally, in practice FSLEs have been shown to be a useful heuristic in identifying flow manifolds in two-dimensional data. In effect, the FSLEs here represent the emergent structures one would expect to see if the larger-scale mesoscale features visible by satellite were important.

The altimetry-derived currents produced by CLS/CNES were also used to calculate Lagrangian particle trajectories both backward and forward in time, through the use of the Lagrangian diagnostic tool ARIANE (Blanke and Raynaud, 1997; Blanke et al., 1999; Blanke, 1997). Generally, this tool uses either model or empirical output to drive particle trajectories. Since the dominant tracer in this study, chl-*a*, is reactive, the initial point for integration of trajectories for ARIANE was somewhat subjective. As a result, we chose here to start when the bloom associated with LDB was at its pinnacle point, namely 6 March, 2015 as judged by satellite data. It is reasonable to assume that seeding Lagrangian particles from this maximal point in the surface bloom gave the best chance that the particles would remain in the sphere of bloom water, and would point to both the potential source of the bloom and its endpoint. Lagrangian particles were spaced $\frac{1}{50}$° (~ 2 km) apart within the chl-*a* contour of 0.3 $\mathrm{mg\ m^{-3}}$.

3 Results

3.1 Chl-*a* and density distribution and timeseries

3.1.1 MVP Observations

The four MVP transects conducted before and after LDB are shown in Fig. 2. The distributions of chl-*a* fluorescence and isopycnals are presented in panels Fig. 2b-e. During T1 (Fig. 2b), the chl-*a* maxima was initially located near 120 m depth, where it was then present at 100 m before being found at the surface near 77 km, inside the patch. Within the patch, a surface signal was present from the surface to 40 m, with a diminished DCM at 80 m. Outside the patch, at 127 km, the DCM was again found near 120 m.

T2 (Fig. 2c) demonstrated a similar pattern, with the DCM found from 120 to 100 m again, reaching the patch edges at 110 and 222 km. The DCM within the patch was less distinct from the surface signal, while the strongest chl-*a* values were still located within the top 40 m. T3 (Fig. 2d), which followed the same route as T2 but occurred some hours later and in the opposite direction, showed the same structure: a 40 m surface patch located at 22 and 123 km that was not distinct from the DCM, with the DCM found again at 100 and then 130 m by the end of T3, outside the bloom.

The distribution in T4 (Fig. 2e) was sampled a week after T1-T3 and subsequent to station LDB. The bloom was present from 17 to 110 km along T4. In this case, a separate DCM at 70 m was present below the surface signal. Unlike previous transects, the DCM dropped abruptly to 140 m at 90 km, well before the end of the surface bloom at 110 km.

MLD and density contours throughout these transects were relatively flat, with the MLD centered around 19 m and the 22, 23, 24, and 25 density anomaly contours centered at 16, 41, 83, and 182 m, respectively. Among these isopycnals, only the 22 contours reached above the first depth detected by the MVP at 10 m. All of these outcroppings occurred either within the bloom area or adjacent, with the exception of the last at the end of T4.

3.1.2 CTD timeseries

The chl-*a* structure of LDB, as observed during the 47 CTD casts, is shown in Fig. 3. From the beginning until 18 March, the maximum value of chl-*a* could be found between the 22 and 23 density anomalies, around 30-40 m. After 18 March, the chl-*a* max was found at a deeper position near 60 m. Over time, the chl-*a* max deepened, and was found between the density anomaly contours of 23.5 and 24, or 60-80 m depth. From 18 March onward, the surface concentration of chl-*a* also decreased, whereas the chl-*a* max concentration increased and began to resemble a typical DCM distribution. Oscillations in the surface chl-*a* during the first half of the timeseries appear, likely due to non-photochemical quenching.

Throughout LDB, the density anomaly contours remained relatively flat. The 22 isopycnal did not outcrop near the surface, unlike that seen in the MVP transects, though the position of LDB within T2 and T3 was inside the region where the 22 isopycnal was found at a similar depth. Upward and downward oscillations of isopycnals indicated the presence of near-inertial oscillations, which was reflected in the SADCP timeseries that is investigated further in (de Verneil et al., this issue). The MLD, though not formally tied to an isopycnal value, also largely reflected these oscillations. Nitracline depth, which in

our formulation was tied to the 24.34 isopycnal, was consistently found between 100 and 120 m throughout the dataset, well below the chl-*a* max and general bloom area, even when the DCM distribution began to appear towards the end of LDB.

3.2 Physical and biogeochemical water properties

Observations of SD12, LDB, and SD13's water structure and biogeochemical properties are presented in Fig. 4. The three stations had similar temperature and salinity profiles, as indicated in the T-S plot of the upper 200 m (Fig. 4a). All three stations covered a similar density range, with slight variation in their salinities. At the surface, SD12 had slightly lower salinity, while LDB and SD13 overlapped more. At depth, however, SD12 and LDB had closer salinity values, with SD13 showing a salinity maximum at depth.

The nitrate profiles of all three stations (Fig. 4b) showed concentrations near the quantitative threshold limit of the measurement method above 100 m. SD12's nitrate increased the fastest, starting at 100 m whereas LDB and SD13 matched each other, both increasing at 120 m. The different depths at which nitrate began to increase are similar to the DCM present at both SD12 and SD13 (Fig. 4c), with the DCM near 100 and 120 m, respectively. The chl-*a* profiles for the beginning and end of LDB reflected the changes shown in Fig. 3. Phosphate concentrations (Fig. 4d) for all three stations were nearly equal at 85 m depth, and generally increased with depth. Above 85 m however, the concentration decreased for SD12 approaching the surface, though it was always above the quantitative measurement threshold. LDB demonstrated a similar decline in phosphate near the surface, but the values were consistently below the detection limit in the top 40 m. By contrast, phosphate values for SD13 were near a steady concentration up to the surface.

3.3 In situ Ri and Ri_g

The possible presence of balanced, submesoscale currents in the in situ MVP and SADCP datasets was determined by comparing Ri and Ri_g. Since both Ri and Ri_g span several orders of magnitude, $\log_{10}Ri$ and $\log_{10}Ri_g$ during T4 are shown in Fig. 5. All the transects contained similar distributions, and T4 was chosen because of the sharp gradients in chl-*a*. The majority of observations of $\log_{10}Ri$ and $\log_{10}Ri_g$ were above 0, or 1 in normal space, and so here we diagnosed that the circulation was largely not submesoscale in its dynamics. $\mathrm{Log}_{10}Ri$ (Fig. 5a) values were similar to but slightly lower than $\log_{10}Ri_g$ (Fig. 5b), demonstrated by a preponderance of saturated shading in 5b. Larger $\log_{10}Ri_g$ values were found at depth, with the smallest $\log_{10}Ri_g$ found near the surface. In the top 50 m, the mean of $\log_{10}Ri_g$ was 1.38, whereas it was 1.54 for the entire profile. By contrast, $\log_{10}Ri$ was more consistent between the top 50 m and all depths, with a mean of 1.35 and 1.36, respectively. Only 2.2% of $\log_{10}Ri_g$ was less than or equal to 0, with 6% for $\log_{10}Ri$. Additionally, for values less than or equal to 1, 39% and 35% of $\log_{10}Ri_g$ and $\log_{10}Ri$, respectively, reached these levels for all depths. Ri reached a minimum near the surface for the last 40 km of T4, which was not reflected in Ri_g. Some structures in Ri appeared in a diagonal orientation, such as between 75 and 125 km at 100 m depth. Vertical patterns appeared in Ri_g, spanning approximately 10 km horizontally, where several isopycnals were concurrently found closer to the surface or deeper. One clear example of this occurred near 25 km within the upper 50 m. Beyond the minimum Ri values at the surface near the end of T4, there were no distinguishing features for either Ri or Ri_g between being inside the chl-*a* bloom and outside, neither at the surface nor at depth.

3.4 Satellite chl-*a* timeseries, altimetry-derived FSLE, and ARIANE trajectories

The remotely sensed distribution of surface chl-*a*, calculated FSLEs and ARIANE Lagrangian particle positions, over a period spanning 25 December, 2014 to 10 May, 2015 are shown in Fig. 6. FSLEs and particles are shaded gray and red, respectively, with 10 % of the particles randomly selected for plotting in all subpanels. 25 December (Dec., all months hereafter shortened) was chosen as the starting point by visually examining the chl-*a* dataset for a pre-bloom period, with a bloom 'source' region identified on 13 Jan. centered at 186° E, 20° S. The temporal evolution of FSLEs and of the Lagrangian particles superimposed on SST is reproduced in Fig. S4 of the Supplementary Material. Additional chl-*a* data, between Jan 10 and 31, 2015, are also provided in Fig. S6.

The 25 Dec. start date showed a modest chl-*a* region oriented North-South (N-S) near 186° E (Fig. 6a) with several likewise N-S oriented FSLEs both inside the chl-*a* region and to the east. Lagrangian particles were dispersed over the northern half of the defined region of interest. On 13 Jan., the identified source region showed the chl-*a* patch localized near an island group located at 20° S, 186° E (Fig. 6b). Multiple FSLE ridges were stacked near the chl-*a* patch, indicating the likely flow along these trajectories to the east. Additionally, another ridge appeared, oriented N-S near 189.5° E, and aligned with a weaker chl-*a* gradient. The Lagrangian particles had now advected west and were flowing south, near the island group 'source' region.

On 31 Jan. (Fig. 6c), the FSLEs to the south of the source island group had evolved into a recirculation pattern to the South, creating a lobe of low chl-*a* water near 20.5° S, 187° E. The ridge near 189.5° E on 13 Jan. had moved westward, and collided with the eastward-flowing chl-*a*, creating a N-S stretching of the bloom. The northward flowing arm of the bloom now approached an East-West (E-W) FSLE ridge (17°S, 187° to 189° E). At this time, the particles had likewise begun to move from the island group to the east, with some particles overlapping the high chl-*a* bloom.

By 16 Feb. (Fig. 6d), the E-W FSLE ridge was now slanted, as was the chl-*a* patch's northern boundary. To the south, the FSLE ridge that collided with the patch on 31 Jan. had begun to move west, as had the chl-*a* patch spanning 22° to 20° S, 187° E. High chl-*a* concentrations positioned at 18.5° S, 189° E had advected eastward between the gap in the E-W FSLE ridge and the N-S ridge that collided with the bloom near 31 Jan. The Lagrangian particles were mostly within the elevated chl-*a* region, and like the bloom water they largely did not cross the FLSE ridge.

On 6 Mar. (Fig. 6e and f), the E-W FSLE ridge had stabilized the formerly northward flowing bloom waters, and another N-S ridge near 191° E began to move in from the east. Another FSLE ridge embedded within the southern bloom lobe positioned near 20° S, 187° W, indicated possible strong flow inside the bloom itself. More E-W ridges at 21° S, 188°, E also appeared near the bloom's southern boundary. Farther south, apart from the current bloom of study, bands of high and low chl-*a* water appeared amidst E-W FSLE structures. These structures were more or less present from this point on until the end of the study period. Lagrangian particles for 6 Mar. were all located within the high chl-*a* region since this was the chosen particle initialization time.

By 21 Mar. (Fig. 6g), the day of MVP T4 sampling, the N-S ridge from earlier had collided with bloom waters and stopped their eastward transit (18° S, 191° E). The circulation inside the bloom, coinciding with a ridge from 20° to 18° S, 188° E, had entrained low chl-*a* water near the former center of the bloom, producing two lobes of high chl-*a* regions to either side. The

particle distribution likewise had these two lobes, and the southern particles had begun to move west, beginning the shearing apart of the chl-*a* bloom.

3 Apr. (Fig. 6h) began to show the general decrease in chl-*a*, a trend that continued until 24 Apr. and 10 May (Fig. 6i-j). The N-S FSLE values near T4 on 21 Mar. (now 18° to 19° S, 189° E) had advected westward, along with the recirculation ridge (20° to 17° S, 187.5° E) and the remnants of the bloom at LDB. Particles had now spread apart, largely overlapping the decreasing chl-*a* bloom and oriented along FSLE ridgelines. Another E-W ridge (17.5° S, 189°-190° E) asserted itself by 24 Apr., oriented along a new post-bloom boundary between moderate and low chl-*a* values. 10 May, the end of this study period, now had a region of minimum chl-*a* in the exact region where the bloom was near its peak chl-*a* satellite values on 6 Mar. (compare Fig. 6f and j). Numerous N-S and E-W ridges, generally aligned with the remnant chl-*a* gradients, continued to move west, along with particles generally embedded within them.

Statistical properties of the Lagrangian particle positions and their respective chl-*a* values are presented in Fig. 7. The percentage of Lagrangian particles that stayed within the study region is shown in Fig. 7a. Throughout the entire period of consideration, the percentage of particles within the region was always greater than 70%. During the backward integration, over 95% of the particles were present until 13 Jan., the date when the bloom was localized near the island group. Prior to this date, the percentage dropped until it was near 70% on the first day, 25 Dec., 2014. In the forward integration, the proportion of particles steadily dropped, until it was around 80% in early to mid-April, after which it rose. The downward trend slowly reasserted itself, and by 10 May, the end of the period, the percentage had dropped to near 70% like in the backward integration.

The mean value of chl-*a* at the particle positions is depicted along with the mean satellite value, as well as the 1, 25, 75, and 99% satellite values in Fig. 7b. Moving in either direction from the 6 Mar. starting point, the mean particle chl-*a* concentration dropped from its initialization peak. The particle mean chl-*a* value was consistently above the mean satellite value, except for a short period at the end of the backward integration in Dec. 2014. Particle mean values reached the 75% threshold 16 Feb. and 3 Apr. in the backward and forward integrations, respectively. The satellite 99% value rose from Dec. 2014 to 13 Jan., when the bloom was identified near the island group. The 99% value varied around this point until reaching its maximum shortly after 6 Mar., the initialization date for the particle experiments. After this point, the 99% satellite value began to decline, with a precipitous drop after 21 Mar., the date of MVP T4.

4 Discussion

4.1 Chl-*a* bloom processes, physical forcing, and collapse

The bloom sampled in this study had a number of distinguishing features that differentiate it from the surrounding water sampled during OUTPACE. Together with physical measurements, these characteristics allow for a determination of what combination of biogeochemical processes and physical forcing were responsible for the bloom and its temporal evolution.

Since this study focuses on a surface bloom, there must be some process responsible for the relative accumulation of chl-*a*. Ideally, in situ biological rate measurements would have been measured before and during the chl-*a* increase. In addition to the pragmatic difficulty of obtaining all these measurements for all time and space, the satellite data suggest the bloom was already

two months old by the time of sampling at station LDB, precluding direct observation of its initial conditions. Therefore, one must start with the assumption that the starting conditions for the bloom were similar to surrounding regions (eg the chl-*a* distribution pre-bloom on 25 Dec., Fig. 6a). We can infer, then, that the local increase of chl-*a* in the bloom was linked to a source of new production. For the WTSP, the two main mechanisms to consider are first nitrate delivery from below due to advective fluxes and/or diapycnal mixing, and secondly N_2 fixation by diazotrophs.

The data from stations SD12, LDB, and SD13, support the role of N_2 fixation in creating the bloom and reject nitrate delivery from below. Firstly, the high chl-*a* concentrations in the bloom were located in the top 40 m, as shown by the in situ MVP surveys (Fig. 2) and station LDB CTD timeseries (Fig. 3). The nitracline, one potential source for new production, was consistently at least 60 m deeper in the water column in the CTD timeseries than the bloom. In order to provide an advective flux, the isopycnals present would have at some point needed to traverse the nitracline depth to the bloom at the surface. This did not occur anywhere within the CTD timeseries. Additionally, the only isopycnal that outcropped during the MVP transects passing inside and outside of the bloom, the 22 $\mathrm{kg\ m^{-3}}$ anomaly, normally resided in the upper 30 m. Therefore, the stable stratification and lack of horizontal density gradients spanning the top 100 m rule out the potential for a vertical advective flux of nitrate to the surface bloom. These observations do not preclude the possibility that an initial nitrate flux occurred two months prior during the bloom's inception, with the water column subsequently mixing and re-stratifying. This possibility is highly unlikely, considering that stations SD12 and SD13 had similar T-S characteristics and nitrate profiles to LDB, and yet had a DCM instead of a surface chl-*a* bloom (Fig. 4). These data therefore also remove the possibility of a massive diapycnal mixing event.

~~The lack of~~ Similar surface blooms in oligotrophic regions have been investigated before, with varying mechanisms to explain their initiation. In particular, upwelling due to mesoscale frontogenesis and wind forcing, are possible causes for surface blooms (Calil et al., 2011; Law et al., 2011). While there are no in situ data during the bloom's appearance in mid-January 2015, sufficient data exist to judge these mechanisms, which would provide advective flux and diapycnal mixing, respectively. Upwelling due to mesoscale frontogenesis can be diagnosed using the Omega equation (Hoskins et al., 1978) with the assumptions employed by Calil et al. (2011) for its use with altimetry data. Calculating this forcing for the OUTPACE bloom resulted in values three orders of magnitude smaller than those for the 2008 bloom of Calil et al. (2011) (Fig. S7). As further comparison, climatological data from station ALOHA in that study place phosphate reservoirs for N_2 fixation at 40 m depth, shallower than the depths observed during OUTPACE. These results, in addition with the lack of SST gradients one would expect (Fig. S4), make this mechanisms unlikely.

Another mechanism is strong wind forcing, such as that provided by tropical cyclones. These storms have been shown to fertilize blooms in oligotrophic waters (Law et al., 2011). Using the value-added altimetry dataset with wind component, the impact of wind was evaluated and found to be relatively small (Fig. S8) and could not create deep mixing. By contrast, another region in the OUTPACE domain witnessed the passage of Cyclone Pam in early March 2015. The satellite imagery before and after its passage corroborate the fertilizing effect of storms in this region (Fig. S9). Whereas the LDB bloom lasted for over two months, this increase in chl-*a* lasted approximately a month. Therefore, given the lack of strong forcing, a mechanism must be invoked that can produce blooms of greater magnitude and duration than those produced by passing storms.

The lack of evidence for mixing events or advective nutrient fluxes leads us to consider the parsimonious alternative that the bloom was supported by N_2 fixation as the source of new production. Diazotrophs, the organisms responsible for N_2 fixation, are normally concentrated in the surface layer ~~, exactly where the~~ in sufficiently warm water ($\geq$ 25 °C threshold in Calil et al., 2011). The LDB bloom was found ~~, and during station LDB~~ in the upper surface layer, satellite SST was warmer than the 25° C threshold for its entirety (Fig. S10), and finally this process was observed directly (Caffin et al., this issue). Evidence for N_2 fixation's role was also reflected in the nutrient profiles. Nitrate levels in the top 100 m were consistently below the quantitative threshold, unsurprising since nitrogen is normally the limiting nutrient. Once nitrogen fixation relieves nitrogen limitation at the surface, other inorganic nutrients such as phosphate are consumed. The decreasing concentration of phosphate near the surface at station LDB, as opposed to the constant values at station SD13, supports this interpretation. Interestingly, station SD12 showed a similar decrease, yet not as strongly. This allows for the possibility that stations SD12 and LDB were more alike in the fact that at some point N_2 fixation was occurring in situ, though the DCM structure at SD12 and SD13 resembled each other more. The possibility that SD12 also hosted nitrogen fixation, whereas SD13 did not, fits within the overall, regional gradient in nitrogen fixation that OUTPACE set out to observe going toward the SPG. For the purpose of this study, it is sufficient to note that the extent of nitrogen fixation present at LDB was likely much larger than at SD12 and in surrounding waters, considering the observed phosphate depletion and the long-lived surface chl-*a* signal associated with the bloom.

Station LDB's CTD timeseries also showed the decrease of surface chl-*a* and the new formation of a DCM near 80 m. Fluctuations in the surface chl-*a*, a possible artifact of non-photochemical quenching, were small in relation to the large change in chl-*a* that occurs between the first and second halves of the timeseries. MVP T4 likewise showed the concurrent surface bloom and the appearance of a DCM at 70 m immediately after station LDB. As previously mentioned when considering nutrient delivery from below, the relatively flat isopycnals also precluded the reverse movement, namely physical subduction of chl-*a* away from the surface. Instead, other mechanisms must be considered. The passive movement of chl-*a* from the surface to a DCM through sinking was possible, but not likely to be a major sink due to the small cell sizes of the plankton concerned (though TEP may be a factor; (Berman-Frank et al., this issue)). In situ removal of chl-*a* may have occurred for a number of reasons. First, the exhaustion of phosphate at LDB may have led to a decline in production, which could not match the removal processes of senescence and grazing. Indeed, dissolved inorganic phosphate (DIP) turnover times reached 0.1-0.2 days above 40 m depth, a value largely below the critical value of 2 days necessary for *Trichodesmium* spp., a major N_2 fixer in this area, to grow (Moutin et al., 2005). Second, the bloom may have fallen victim to increased predation, as abundance of some zooplankton was enhanced (Dolan et al., 2016). Interestingly, even though these biological mechanisms are mediated in situ by planktonic organisms, the regional and simultaneous collapse of the bloom was documented by satellite imagery (Fig. 6 g-h), meaning the same mechanisms most likely acted throughout the bloom. The chl-*a* structure at the end of station LDB resembled that of SD12 much more than its initial distribution at the beginning. This observation, in conjunction with evidence of nitrogen fixation near the surface, raises the possibility that at some point station SD12 underwent a similar process, and that surface blooms may play a more general role in the region.

4.2 Surface circulation, chl-*a* advection, and the formation of gradients

The major focus of this study, apart from diagnosing the bloom's biogeochemical makeup, is to identify which circulation patterns explained the horizontal distribution of the bloom once it was formed, namely submesoscale or mesoscale currents. Comparing the in situ datasets with satellite altimetry currents, the relevant scales of surface motion in the WTSP can be deduced.

As mentioned in the introduction, though the SEC is the mean current advecting water westward from the northern limb of the subtropical gyre, much more kinetic energy is typically found at the mesoscale. Interest has mounted in recent decades in the possibility that submesoscale currents, intensified at the surface, may play a role in affecting nutrient delivery into the euphotic zone, as well as redistributing biological tracers, including in N_2 fixation zones (Calil and Richards, 2010). While nutrient delivery has been ruled out for this particular bloom, there remains the possibility that submesoscale motions played a role in the lateral advection of the surface bloom, as well as providing the shear necessary to form the strong chl-*a* gradients observed in the MVP transects. In particular, recent findings highlight both the seasonal (Callies et al., 2015) and geographic (Callies and Ferrari, 2013) occurrence of submesoscale turbulence; for the WTSP, it is unclear whether it should be favored or not. On one hand, it is located away from regions of strong baroclinic currents such as western boundary currents, and according to eq. (2) the reduced Coriolis parameter relative to temperate latitudes should slightly reduce the geostrophic Ri_g. Conversely, the late summer stratification may inhibit these motions, making the end result of these competing effects difficult to predict a priori.

The values of Ri and Ri_g present within the top 50 m of the MVP transects were predominantly greater than 1, with the majority larger than 10 (0 and 1 in log-space, respectively). Considering these two independent measurements of shear agreed in magnitude, and that both occurred outside the dynamical range of consideration, the data thus provided little support for the presence of submesoscale circulation, perfectly balanced or otherwise.

Combining the strong surface stratification, general lack of isopycnal outcroppings (ie no strong horizontal density gradients), and absence of correspondence between chl-*a* and density gradients, it should perhaps not be surprising that buoyancy-driven submesoscale circulation was not readily discernable even at the surface in this dataset. If most submesoscale structures are expected to be in the mixed layer, which throughout this dataset was near 20 m, then the sub-kilometer Rossby radius R_D (here found to be < 200 m) would not have been resolved by the MVP survey ~~.~~since MVP horizontal resolution is ~ 2 km. Besides problems of horizontal resolution, the shallow mixed layer also precluded complete vertical resolution by the underway MVP. As a result, though the summertime conditions present during the surveys lend support to reduced submesoscale circulation, the very same conditions make it difficult to state with confidence that the Ri and Ri_g methodology is entirely conclusive. However, since the bloom of interest in these surveys spanned the top 40 m, and covered hundreds of kilometers in horizontal extent, these small features, should they have existed, would not have impacted the full depth range of the bloom, nor would they have significantly affected the horizontal advection of the entire bloom. Furthermore, the strongest gradient in chl-*a* found in MVP T4 had no visible density structure at these scales to suggest a source of horizontal shear to create this gradient.

The possibility remains that during other periods of the year such as winter, with a deeper mixed layer than that observed during the cruise, the horizontal spatial scales of these features would increase and possibly impact the advection of such a bloom. The question thus becomes whether these bloom events occur during winter periods. If not, then the mutually exclusive timing of bloom events and stratification favorable for submesoscale turbulence would preclude its influence on bloom evolution for the region.

The natural horizontal scales of the bloom were more in line with the R_D of the entire water column, ~ 60 km, which is impacted by the mesoscale regime. In our dataset, satellite altimetry-derived currents represented the mesoscale circulation. Whereas the MVP T4 transect revealed no submesoscale source of horizontal shear to create a chl-*a* gradient, the mesoscale circulation did via an FLSE structure present near MVP T4 in Fig. 6g. While FSLEs may not provide the exact regions where chl-*a* gradients form in the station LDB bloom, they help define dynamical boundaries that provide more explanation than the in situ data for why the chl-*a* bloom appeared as it did.

The positions of Lagrangian particles also allow for a better representation of where bloom water advected, as shown in Fig. 7. Firstly, most particles were present in the defined region of interest throughout the timeseries (Fig. 7a), providing additional support (beyond visual inspection) that the chl-*a* dataset sufficiently covered bloom water relative to the chosen initial time of integration, March 6. If the chl-*a* satellite timeseries therefore encompasses most of the bloom water of interest, then the fraction of particles in high chl-*a* water throughout their trajectories, as represented in Fig. 7b, is an indication of the performance of these particles in keeping with the bloom. Evidently, chl-*a* is a reactive tracer and undergoes its own evolution, as shown by the shaded areas in Fig. 7b. ~~The~~ By contrast, the temporal evolution of SST, which does not suffer from this deficiency, did not display enough variability in the bloom region to confirm the efficiency of FSLEs or ARIANE particles in representing its advection (Fig. S4 in the Supplementary Material). This is most likely due to the strong, regional summertime heating that occurs at these latitudes. Moreover, the particle positions are not reliable over long timescales. Few particles can be found in the bloom on Jan 13, when it was localized near a group of islands. Conversely, a second initialization experiment on Jan 13 failed to produce many particles in the bloom for Mar 06 and Mar 21 (Supplementary Material, Fig. S5). This limitation may be a result of chl-*a* being reactive or of unresolved motions in the altimetry-derived flow field. Therefore, while the ability of the Lagrangian particles to ~~both~~ remain in the region of interest and to accurately represent elevated chl-*a* values (mostly above or near the 75th percentile) provides ~~strong~~ positive evidence that mesoscale flows were indeed advecting the bloom water~~.~~, after around two months the accumulated errors due to unresolved flows make direct inspection of particle position uninformative. The FSLEs, in comparison, do not suffer from this sensitivity.

With accurate representation of the advection of bloom water, an interesting picture emerges. Firstly, the ~~passage of particles~~ location of the bloom near an island group ~~before and at the beginning of the bloom~~ on Jan 13 (Fig. ~~6a-b~~6b, S5) suggests a possible island effect in the ignition of the bloom. Despite the fact the bloom's beginning was not captured by in situ data, we still suggest a mechanism responsible for causing the bloom. Considering that N_2 fixation drove new production, and nearby stations SD12 and SD13 had detectable phosphate levels, alleviation of another necessary and limiting nutrient, iron, was possibly at work. The enrichment of diazotrophs near island inputs, and their subsequent advection (along with their primary production), has been documented previously (Dupouy et al., 2013; Shiozaki et al., 2013). Secondly, the shifting

FSLEs and ~~Lagrangian particle tracks~~ both Lagrangian particle experiments (Figs. 6, S5, and S6) demonstrate the general eastward advection of the bloom from its localized island source in Fig. 6b until its easternmost position in Fig. 6g. This eastward evolution is not what one would expect a priori. Indeed, both the SEC, as well as the mesoscale structures responsible for currents in the altimetry dataset, propagate westward, reflected by the migration of N-S oriented FSLE ridges the bloom encountered in Fig. 6b-d and Fig. 6f-g.

Therefore, the complex circulation evoked by a westward-moving mesoscale field allowed for the counterintuitive eastward advection of water with enhanced biological production at its surface. This was possible due to the bloom occurring in water not associated with the coherent, elliptic structures that move west~~, and which are what most investigators focus on for mesoscale transport~~. Instead, the bloom occurred in water outside these structures, with tortuous trajectories hyperbolic in nature ~~(Kirwan et al., 2003)~~(Kirwan et al., 2003; Rypina et al., 2010). Eventually, as the bloom collapses, more particles move west with the mean circulation, as shown in Fig. 6h-j. The temporal overlap between the surface bloom's occurrence and maintenance until its collapse, in conjunction with its easternmost transport, is possibly a coincidence. It does suggest, however, the important role that complex mesoscale flows outside of coherent, elliptic eddies have in determining where new production eventually ends up.

5 Conclusions

In this study, we document a surface chl-*a* bloom observed in the WTSP spanning two months from mid-January until mid-March 2015. Large-scale in situ surveys conducted by an MVP platform both confirm the surface signal seen by satellite and further show the lack of the DCM common in the region. A quasi-Lagrangian CTD timeseries additionally shows the collapse of the surface bloom, also corroborated by satellite. Through the use of chl-*a*, density, and nutrient profiles, the delivery of nutrients from depth is ruled out as a mechanism sustaining the bloom. Instead, the surface bloom hosted significant N_2 fixation as a source of new production. In the WTSP, the hotspot for N_2 fixation in the world, the surface inorganic phosphate from the South Pacific gyre may represent an important nutrient source for maintaining such blooms subsequent to sufficient introduction of iron, possibly due to island effects.

The circulation responsible for advecting the bloom at the surface was satisfactorily represented by altimetry-derived mesoscale currents, with physical structures corresponding to biological gradients. The in situ density and velocity data, in contrast, did not have structures that correspond with the sharp gradients in chl-*a*. Additionally, the dynamical nature of the in situ data did not fall within the submesoscale regime. In the ongoing debate between the seasonal and geographic distribution of submesoscale turbulence, this dataset posits the first-order importance of mesoscale circulation in the WTSP summer. The complex trajectories that mesoscale currents create in hyperbolic regions outside of eddies can be of prime importance in advecting blooms, sometimes in counterintuitive directions such as the eastward transport presented here.

Future studies in the region will be necessary to resolve residing questions. For instance, the particular biogeochemical conditions igniting the bloom, here hypothesized to be island-derived iron, cannot be confirmed within this dataset and will

require further in situ sampling. Additionally, the presence of submesoscale structures during other parts of the year, such as wintertime with deeper mixed layers, remains unanswered.

However, armed with the information that not only summertime blooms fueled by N_2 fixation occur in the WTSP, but that their advection at the surface may be represented by the value-added, high-resolution satellite products such as those produced by CLS/CNES, future studies may begin to quantify the combined inter-annual impact of N_2 fixation and mesoscale transport in distributing new production in this region.

Acknowledgements. We would like to thank the two anonymous reviewers and Associate Editor who helped in making this a better article. This is a contribution of the OUTPACE (Oligotrophy from Ultra-oligoTrophy PACific Experiment) project (Moutin and Bonnet, 2015) funded by the French national research agency (ANR-14-CE01-0007-01), the LEFE-CyBER program (CNRS-INSU), the GOPS program (IRD) and CNES (BC T23, ZBC 4500048836). The OUTPACE cruise was managed by MIO (OSU Institut Pytheas, AMU) from Marseilles (France). The authors thank the crew of the RV *L'Atalante* for outstanding shipboard operations. G. Rougier, M. Picheral, and L. Bellomo are warmly thanked for their help in CTD rosette and MVP deployment and data processing. We also thank A. Gimenez for T_{DIP} measurements, and S. Helias-Nunige for nutrient values. C. Schmechtig is thanked for LEFE-CyBER database management. Satellite SST, Chl-*a*, and altimetry data have been provided by CLS in the framework of CNES funding; we thank I. Pujol and G. Taburet for their support in providing these data. A. Lozingot is acknowledged for administrative aid for the OUTPACE project.

References

Aminot, A. and Kérouel, R.: Dosage automatique des nutriments dans les eaux marines: méthodes en flux continu, Editions Quae, 2007.

Berman-Frank, I., Spungin, D., Belkin, N., Van-Wambeke, F., Gimenez, A., Caffin, M., Stengren, M., Foster, R., Knapp, A., and Bonnet, S.: Programmed cell death in diazotrophs and the fate of C and N in the Western Tropical South Pacific, Biogeosciences, this issue.

Blanke, B.: ARIANE, http://www.univ-brest.fr/lpo/ariane, 1997.

Blanke, B. and Raynaud, S.: Kinematics of the Pacific equatorial undercurrent: An Eulerian and Lagrangian approach from GCM results, Journal of Physical Oceanography, 27, 1038–1053, 1997.

Blanke, B., Arhan, M., Madec, G., and Roche, S.: Warm water paths in the equatorial Atlantic as diagnosed with a general circulation model, Journal of Physical Oceanography, 29, 2753–2768, 1999.

Bonnet, S., Caffin, M., Berthelot, H., and Moutin, T.: Hot spot of N_2 fixation in the western tropical South Pacific pleads for a spatial decoupling between N_2 fixation and denitrification, Proceedings of the National Academy of Sciences.

Bouruet-Aubertot, P., Cuyper, Y., Le Goff, H., Rougier, G., de Verneil, A., Doglioli, A., Picheral, M., Yohia, C., Caffin, M., Lefèvre, D., Petrenko, A., and Moutin, T.: Longitudinal contrast in small scale turbulence along 20° S in the Pacific Ocean: origin and impact on biogeochemical fluxes, Biogeosciences, This issue.

Caffin, M., Moutin, T., Bouruet-Aubertot, P., Doglioli, A., Grosso, O., Helias-Nunige, S., Leblond, N., Gimenez, A., de Verneil, A., and Bonnet, S.: Nitrogen budget in the upper layer of 3 stations "representative" of the Western Tropical South Pacific Ocean: evidence of high nitrogen fixation rates, Biogeosciences, this issue.

Calil, P. and Richards, K.: Transient upwelling hot spots in the oligotrophic North Pacific, Journal of Geophysical Research: Oceans, 115, 2010.

Calil, P. H., Doney, S. C., Yumimoto, K., Eguchi, K., and Takemura, T.: Episodic upwelling and dust deposition as bloom triggers in low-nutrient, low-chlorophyll regions, Journal of Geophysical Research: Oceans, 116, 2011.

Callies, J. and Ferrari, R.: Interpreting energy and tracer spectra of upper-ocean turbulence in the submesoscale range (1–200 km), Journal of Physical Oceanography, 43, 2456–2474, 2013.

Callies, J., Ferrari, R., Klymak, J. M., and Gula, J.: Seasonality in submesoscale turbulence, Nature communications, 6, 2015.

Chaigneau, A. and Pizarro, O.: Mean surface circulation and mesoscale turbulent flow characteristics in the eastern South Pacific from satellite tracked drifters, Journal of Geophysical Research: Oceans, 110, 2005.

Chelton, D. B., Deszoeke, R. A., Schlax, M. G., El Naggar, K., and Siwertz, N.: Geographical variability of the first baroclinic Rossby radius of deformation, Journal of Physical Oceanography, 28, 433–460, 1998.

Chelton, D. B., Schlax, M. G., Samelson, R. M., and de Szoeke, R. A.: Global observations of large oceanic eddies, Geophysical Research Letters, 34, 2007.

Chen, C.-T. and Millero, F. J.: Speed of sound in seawater at high pressures, The Journal of the Acoustical Society of America, 62, 1129–1135, 1977.

Claustre, H., Sciandra, A., and Vaulot, D.: Introduction to the special section bio-optical and biogeochemical conditions in the South East Pacific in late 2004: the BIOSOPE program, Biogeosciences Discussions, 5, 605–640, 2008.

Cotté, C., d'Ovidio, F., Chaigneau, A., Lévy, M., Taupier-Letage, I., Mate, B., and Guinet, C.: Scale-dependent interactions of Mediterranean whales with marine dynamics, Limnology and Oceanography, 56, 219–232, 2011.

de Boyer Montégut, C., Madec, G., Fischer, A. S., Lazar, A., and Iudicone, D.: Mixed layer depth over the global ocean: An examination of profile data and a profile-based climatology, Journal of Geophysical Research: Oceans, 109, 2004.

de Verneil, A., Rousselet, L., Doglioli, A. M., Petrenko, A. A., Bouruet-Aubertot, P., and Moutin, T.: OUTPACE Long Duration Stations: Physical variability and context of biogeochemical sampling, Biogeosciences, this issue.

Doglioli, A. M.: SPASSO, http://www.mio.univ-amu.fr/SPASSO, 2013.

Doglioli, A. M., Nencioli, F., Petrenko, A. A., Rougier, G., Fuda, J.-L., and Grima, N.: A software package and hardware tools for in situ experiments in a Lagrangian reference frame, Journal of Atmospheric and Oceanic Technology, 30, 1940–1950, 2013.

Dolan, J. R., Gimenez, A., Cornet-Barthaux, V., and de Verneil, A.: Community Structure of Tintinnid Ciliates of the Microzooplankton in the South West Pacific Ocean: Comparison of a High Primary Productivity with a Typical Oligotrophic Site, Journal of Eukaryotic Microbiology, 63, 813–822, 2016.

d'Ovidio, F., Fernández, V., Hernández-García, E., and López, C.: Mixing structures in the Mediterranean Sea from finite-size Lyapunov exponents, Geophysical Research Letters, 31, 2004.

d'Ovidio, F., Della Penna, A., Trull, T. W., Nencioli, F., Pujol, M.-I., Rio, M.-H., Park, Y.-H., Cotté, C., Zhou, M., and Blain, S.: The biogeochemical structuring role of horizontal stirring: Lagrangian perspectives on iron delivery downstream of the Kerguelen plateau, Biogeosciences, 12, 5567–5581, 2015.

Dupouy, C., Benielli-Gary, D., Neveux, J., Dandonneau, Y., and Westberry, T.: An algorithm for detecting Trichodesmium surface blooms in the South Western Tropical Pacific, Biogeosciences, 8, 3631–3647, 2013.

Egbert, G. D., Bennett, A. F., and Foreman, M. G.: TOPEX/POSEIDON tides estimated using a global inverse model, 1994.

Ferrari, R. and Wunsch, C.: Ocean circulation kinetic energy: Reservoirs, sources, and sinks, Annual Review of Fluid Mechanics, 41, 253–282, 2009.

Harris, L. D.: Edge effects and conservation of biotic diversity, Conservation Biology, 2, 330–332, 1988.

Hoskins, B., Draghici, I., and Davies, H.: A new look at the ω-equation, Quarterly Journal of the Royal Meteorological Society, 104, 31–38, 1978.

Kirwan, A., Toner, M., and Kantha, L.: Predictability, uncertainty, and hyperbolicity in the ocean, International journal of engineering science, 41, 249–258, 2003.

Law, C. S., Woodward, E., Ellwood, M., Marriner, A., Bury, S., and Safi, K. A.: Response of surface nutrient inventories and nitrogen fixation to a tropical cyclone in the southwest Pacific, Limnology and Oceanography, 56, 1372–1385, 2011.

Le Bot, P., Kermabon, C., Lherminier, P., and Gaillard, F.: CASCADE V6. 1: Logiciel de validation et de visualisation des mesures ADCP de coque, 2011.

Li, Q. P., Franks, P. J., Ohman, M. D., and Landry, M. R.: Enhanced nitrate fluxes and biological processes at a frontal zone in the southern California current system, Journal of plankton research, p. fbs006, 2012.

Longhurst, A. R.: Ecological geography of the sea, Academic Press, 2010.

Mackenzie, K. V.: Nine-term equation for sound speed in the oceans, The Journal of the Acoustical Society of America, 70, 807–812, 1981.

Mahadevan, A.: The impact of submesoscale physics on primary productivity of plankton, Annual review of marine science, 8, 161–184, 2016.

Mahadevan, A. and Tandon, A.: An analysis of mechanisms for submesoscale vertical motion at ocean fronts, Ocean Modelling, 14, 241–256, 2006.

McGillicuddy, D. J., Anderson, L. A., Bates, N. R., Bibby, T., Buesseler, K. O., Carlson, C. A., Davis, C. S., Ewart, C., Falkowski, P. G., Goldthwait, S. A., et al.: Eddy/wind interactions stimulate extraordinary mid-ocean plankton blooms, Science, 316, 1021–1026, 2007.

McWilliams, J. C.: Submesoscale currents in the ocean, in: Proc. R. Soc. A, vol. 472, p. 20160117, The Royal Society, 2016.

Moutin, T. and Bonnet, S.: OUTPACE cruise, RV L'Atalante, doi:10.17600/15000900, 2015.

Moutin, T., Doglioli, A., de Verneil, A., and Bonnet, S.: The Oligotrophy to the UlTra-oligotrophy PACific Experiment (OUTPACE cruise, Feb. 18 to Apr. 3, 2015), Biogeosciences, This issue.

Moutin, T., Van Den Broeck, N., Beker, B., Dupouy, C., Rimmelin, P., and Le Bouteiller, A.: Phosphate availability controls Trichodesmium spp. biomass in the SW Pacific Ocean, Marine Ecology Progress Series, 297, 15–21, 2005.

Moutin, T., Karl, D. M., Duhamel, S., Rimmelin, P., Raimbault, P., Van Mooy, B. A., and Claustre, H.: Phosphate availability and the ultimate control of new nitrogen input by nitrogen fixation in the tropical Pacific Ocean, Biogeosciences Discussions, 4, 2407–2440, 2007.

Moutin, T., Van Wambeke, F., and Prieur, L.: Introduction to the Biogeochemistry from the Oligotrophic to the Ultraoligotrophic Mediterranean (BOUM) experiment, Biogeosciences, 9, 3817, 2012.

Nagai, T., Gruber, N., Frenzel, H., Lachkar, Z., McWilliams, J. C., and Plattner, G.-K.: Dominant role of eddies and filaments in the offshore transport of carbon and nutrients in the California Current System, Journal of Geophysical Research: Oceans, 120, 5318–5341, 2015.

Nencioli, F., Kuwahara, V. S., Dickey, T. D., Rii, Y. M., and Bidigare, R. R.: Physical dynamics and biological implications of a mesoscale eddy in the lee of Hawai'i: Cyclone Opal observations during E-Flux III, Deep Sea Research Part II: Topical Studies in Oceanography, 55, 1252–1274, 2008.

Pedlosky, J.: Geophysical fluid dynamics, Springer Science & Business Media, 2013.

Rousselet, L., de Verneil, A., Doglioli, A., Petrenko, A., Maes, C., and Blanke, B.: Characterization of the mesoscale circulation during the OUTPACE cruise (Western Tropical South Pacific), Biogeosciences, this issue.

Rousselet, L., Doglioli, A., Maes, C., Blanke, B., and Petrenko, A.: Impacts of mesoscale activity on the water masses and circulation in the Coral Sea, Journal of Geophysical Research: Oceans, 121, 7277–7289, 2016.

Rypina, I. I., Pratt, L. J., Pullen, J., Levin, J., and Gordon, A. L.: Chaotic advection in an archipelago, Journal of Physical Oceanography, 40, 1988–2006, 2010.

Shiozaki, T., Kodama, T., Kitajima, S., Sato, M., and Furuya, K.: Advective transport of diazotrophs and importance of their nitrogen fixation on new and primary production in the western Pacific warm pool, Limnol. Oceanogr, 58, 49–60, 2013.

Sohm, J. A., Webb, E. A., and Capone, D. G.: Emerging patterns of marine nitrogen fixation, Nature Reviews Microbiology, 9, 499–508, 2011.

Stammer, D.: Global characteristics of ocean variability estimated from regional TOPEX/POSEIDON altimeter measurements, Journal of Physical Oceanography, 27, 1743–1769, 1997.

Stone, P. H.: On non-geostrophic baroclinic stability: Part II, Journal of the Atmospheric Sciences, 27, 721–726, 1970.

Thomas, L. N., Tandon, A., and Mahadevan, A.: Submesoscale processes and dynamics, Ocean modeling in an Eddying Regime, pp. 17–38, 2008.

Thomas, L. N., Taylor, J. R., Ferrari, R., and Joyce, T. M.: Symmetric instability in the Gulf Stream, Deep Sea Research Part II: Topical Studies in Oceanography, 91, 96–110, 2013.

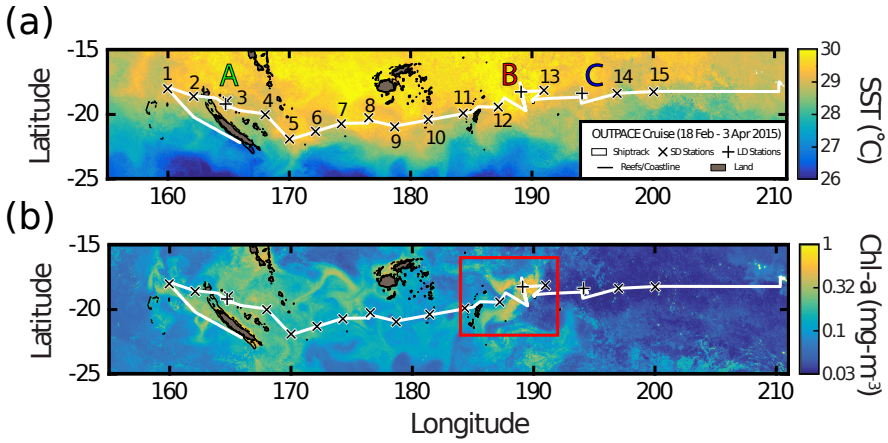

Figure 1. OUTPACE satellite (a) SST and (b) Chl-*a*. Satellite pixel data over 42 days are used to produce a weighted mean. The weight for each pixel is calculated by normalized inverse distance squared from the pixel to the daily mean ship position. The shiptrack, derived from ADCP data, is shown in white, land is shaded gray, with black coastlines and reefs. Short duration (SD) stations are depicted by black X marks, while long duration (LD) stations are shown by black +'s. The LD stations are color-coded, using the convention for the OUTPACE cruise. A red rectangle in the Chl-*a* panel shows the study area for this paper.

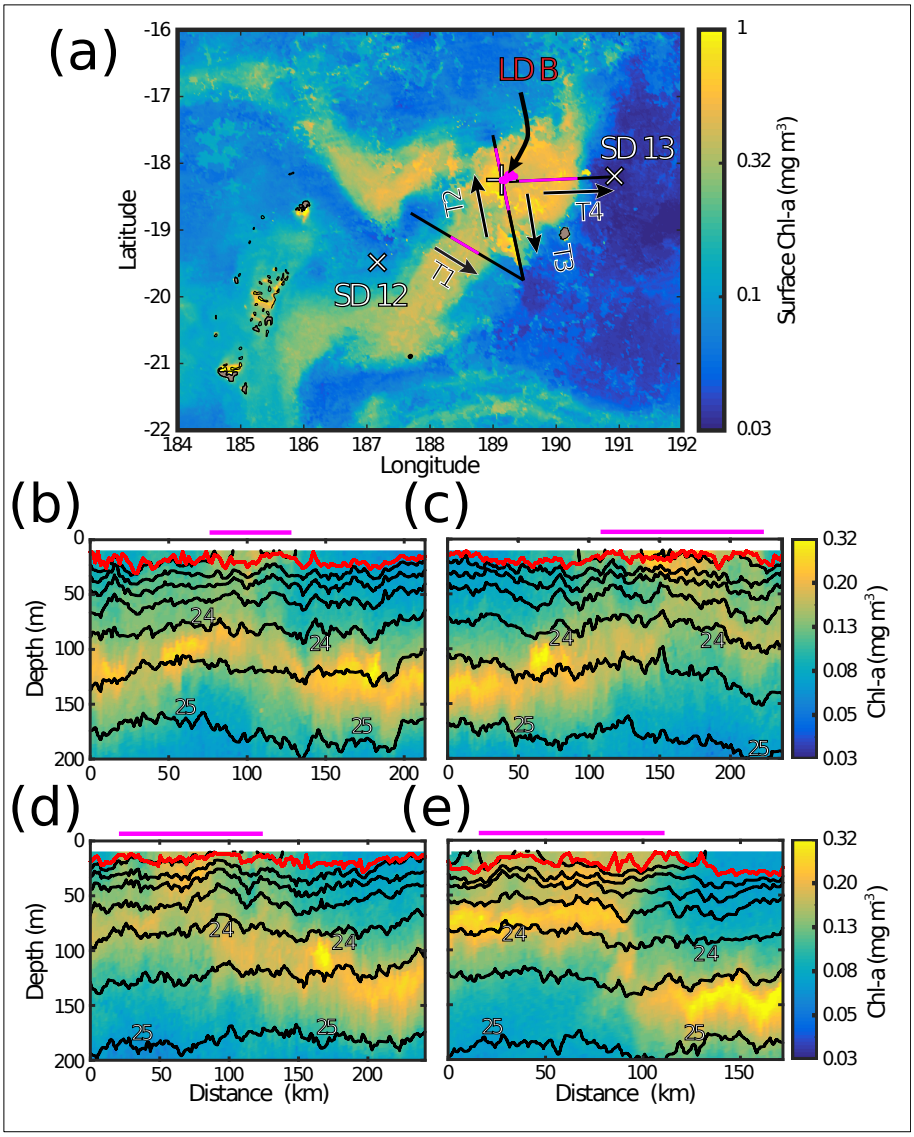

Figure 2. MVP Transects near the station B bloom site. (a) The position of each transect with respect to Chl-*a* fluorescence transects for (b) Transect 1 (T1), (c) Transect 2 (T2), (d) Transect 3 (T3), and (e) Transect 4 (T4). Transect positions are shown by black lines, with the casts designated inside the bloom by MVP data are colored magenta. Stations SD12, LDB, and SD13 are depicted by marks similar to Figure 1. Locations of LDB CTDs are shown in a cluster around the mark designating LDB. Direction of sampling for the transects are shown by arrows. Islands and reefs are also shown in a similar fashion to Figure 1. In situ isopycnals are shown in black, ranging from 22 to 25 $kg - m^{-3}$ in half-steps. The MLD is shown in red, and the magenta brackets above the panels show the casts inside the bloom.

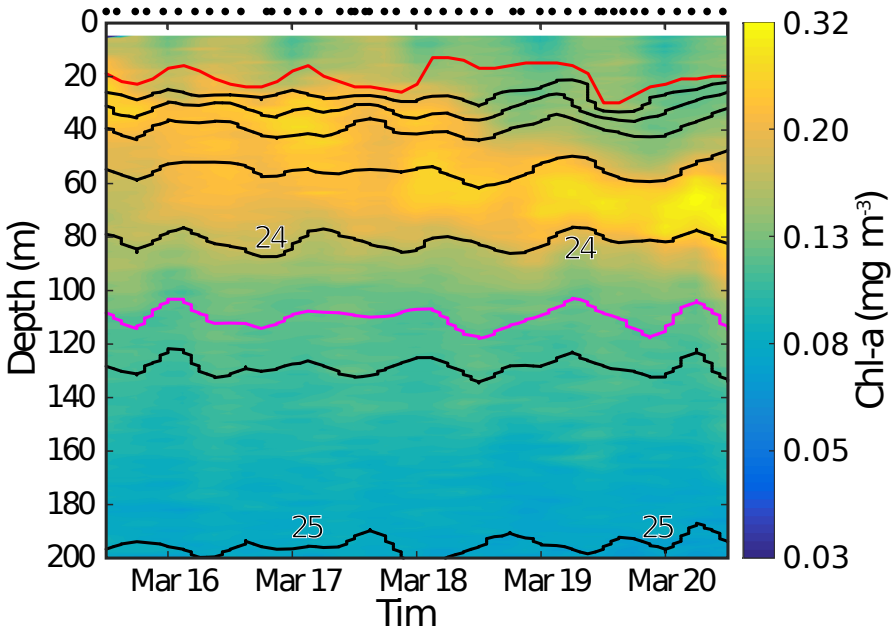

Figure 3. LDB CTD timeseries (in UTC) of Chl-*a*. Contours of density anomaly are superimposed in black ranging from 22 to 25 kg m^{-3} in increments of 0.5. MLD is shown in red, with D_{NO3} in magenta. Black circles above the panel indicate times of CTD casts.

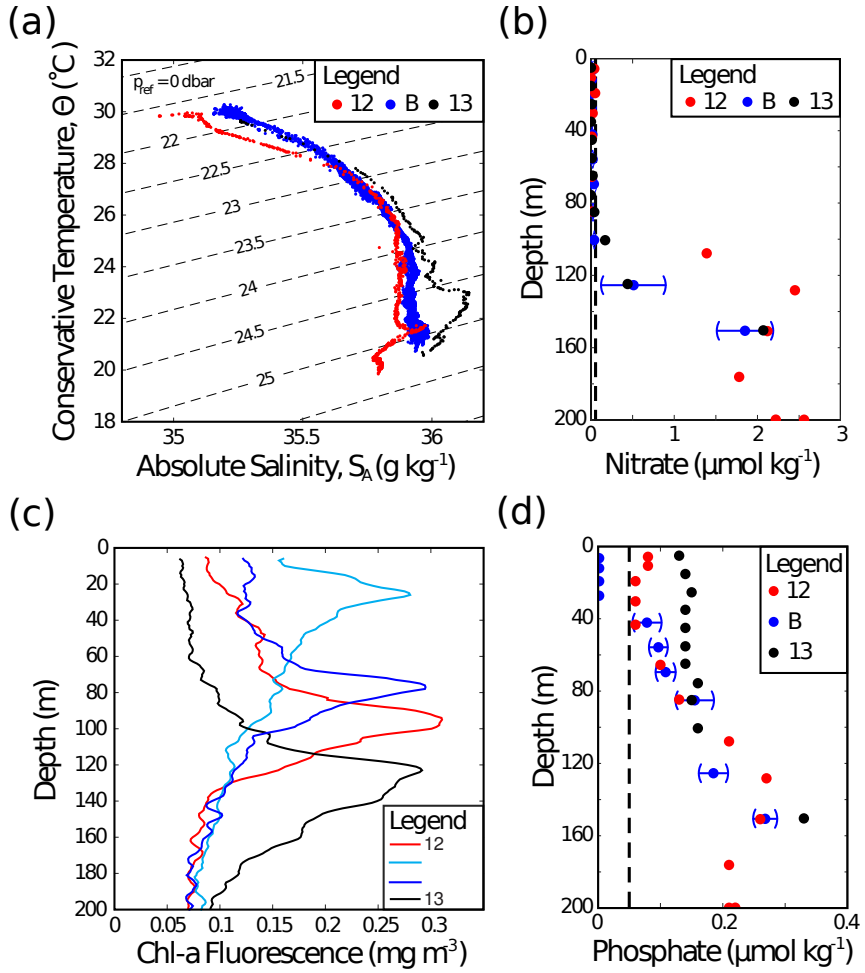

Figure 4. Station SD12, LDB, and SD13 CTD and bottle data. (a) Θ-S_A diagram, (b) NO_3, (c) Chl-a, and (d) PO_4 concentrations. SD12 data is shown in red, LDB in blue, and SD13 in black. Quantitative thresholds for NO_3 and PO_4 are shown by black dashed lines, and any observed values below this threshold are set to 0. The 95% confidence intervals are included for the LDB nutrient values.

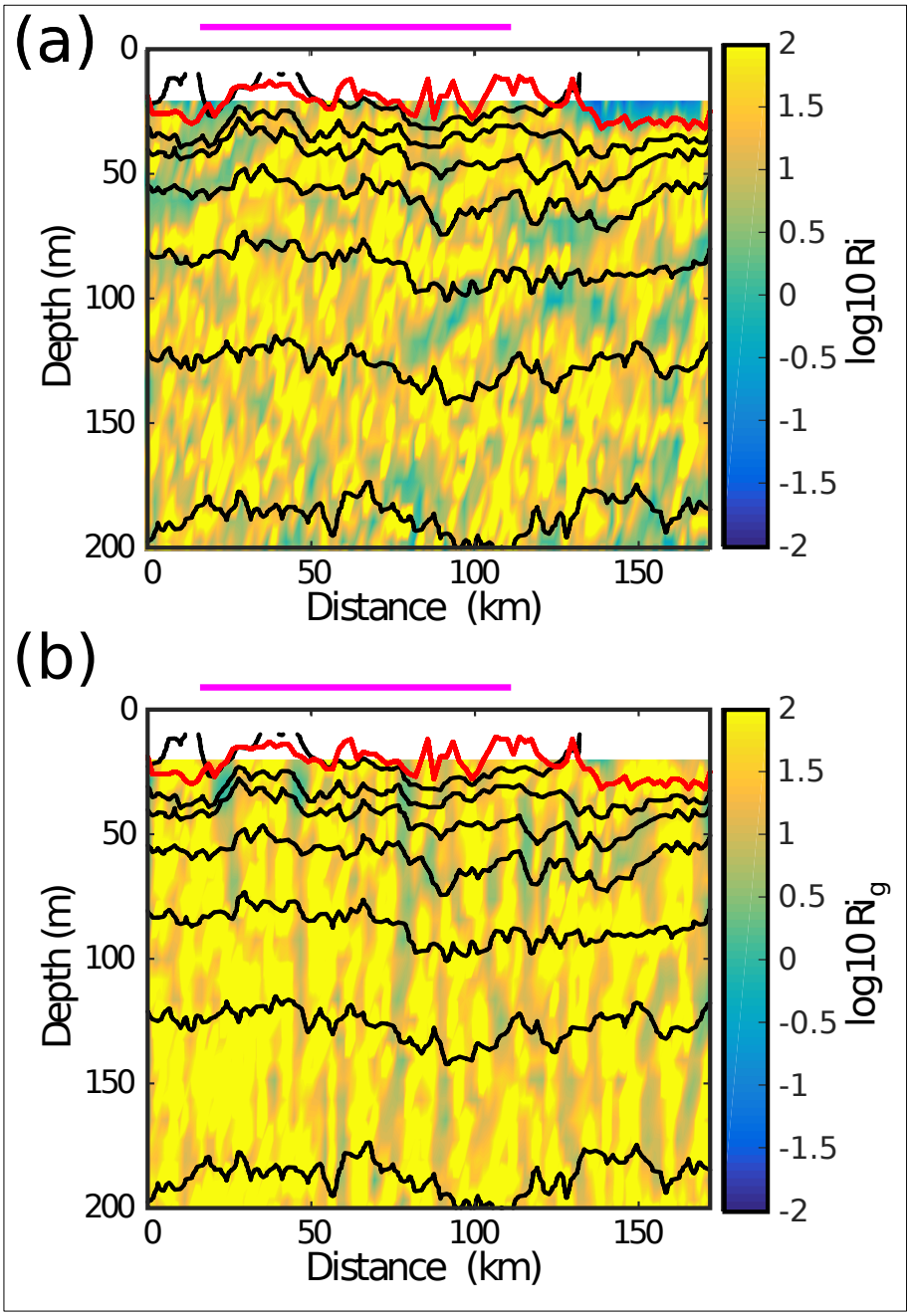

Figure 5. Calculated (a) Ri and (b) Ri_g for MVP T4. Density contours are superimposed in black and MLD in red, with magenta indicating the region inside the bloom, similar to Figure 2e. Please note the log_{10} color scale.

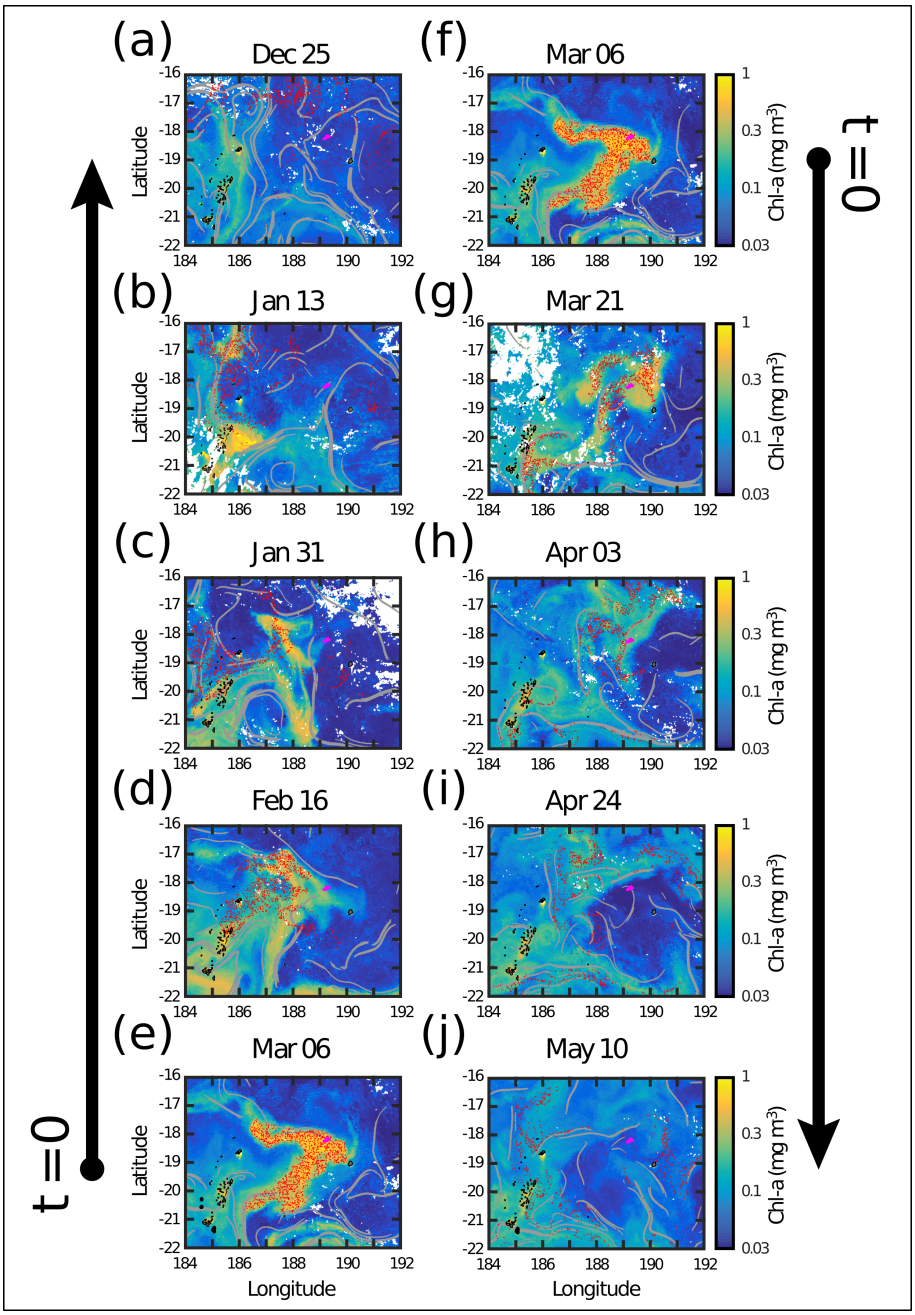

Figure 6. Satellite chl-*a*, FSLE, and ARIANE particles for (a) 25 Dec. 2014, (b) 13 Jan. 2015, (c) 31 Jan., (d) 16 Feb., (e-f) 6 Mar., before station LDB sampling, followed by (g) 21 Mar., the date of MVP T4, concluded by post-bloom (h) 3 Apr., (i) 24 Apr., and (j) 10 May. FSLE values above 0.15 day^{-1} are shaded gray. LDB CTD locations are shown in magenta. A randomly selected subsampling of one-tenth of the ARIANE particles was initially chosen to be shown in red.

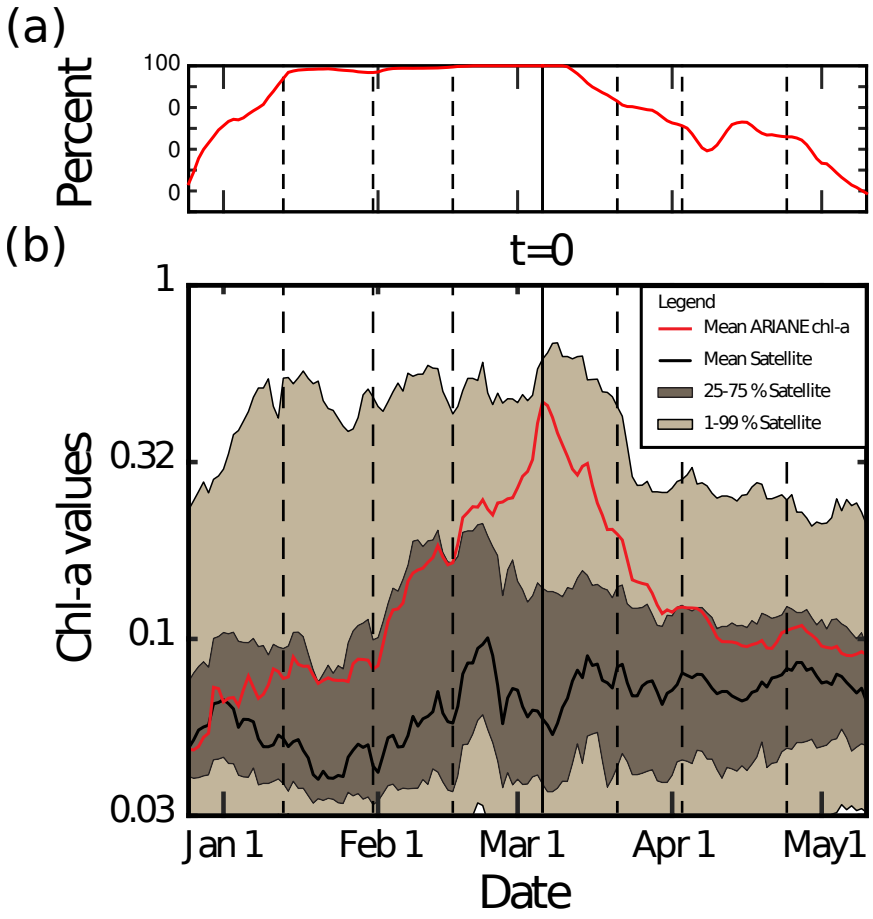

Figure 7. Statistics from ARIANE lagrangian particle trajectories, from Dec 24, 2014 to May 10, 2015, with initial time Mar 6 shown with a solid vertical gray bar, and the dates from figure 6 in dashed lines. (a) Percentage of particles found inside the bloom region, between 184° to 192° E and 22° to 16° S. (b) Mean interpolated chl-*a* value for all lagrangian particles during backward and forward integrations in red, with mean chl-*a* from the CLS dataset in black. Dark shading shows region between 25^{th} and 75^{th} percentiles, with light shading for the 1^{st} and 99^{th}.

Supplementary figures

for "The Fate of a Southwest Pacific Bloom: Gauging the impact of submesoscale vs. mesoscale circulation on biological gradients in the subtropics"

by Alain de Verneil, Louise Rousselet, Andrea M. Doglioli, Anne A. Petrenko, and Thierry Moutin

In the following pages are the refined versions of the figures to be included in the Supplementary Material. We apologize if the captions do not reflect their position in the Supplementary material (eg Fig. S1, S2, etc.)

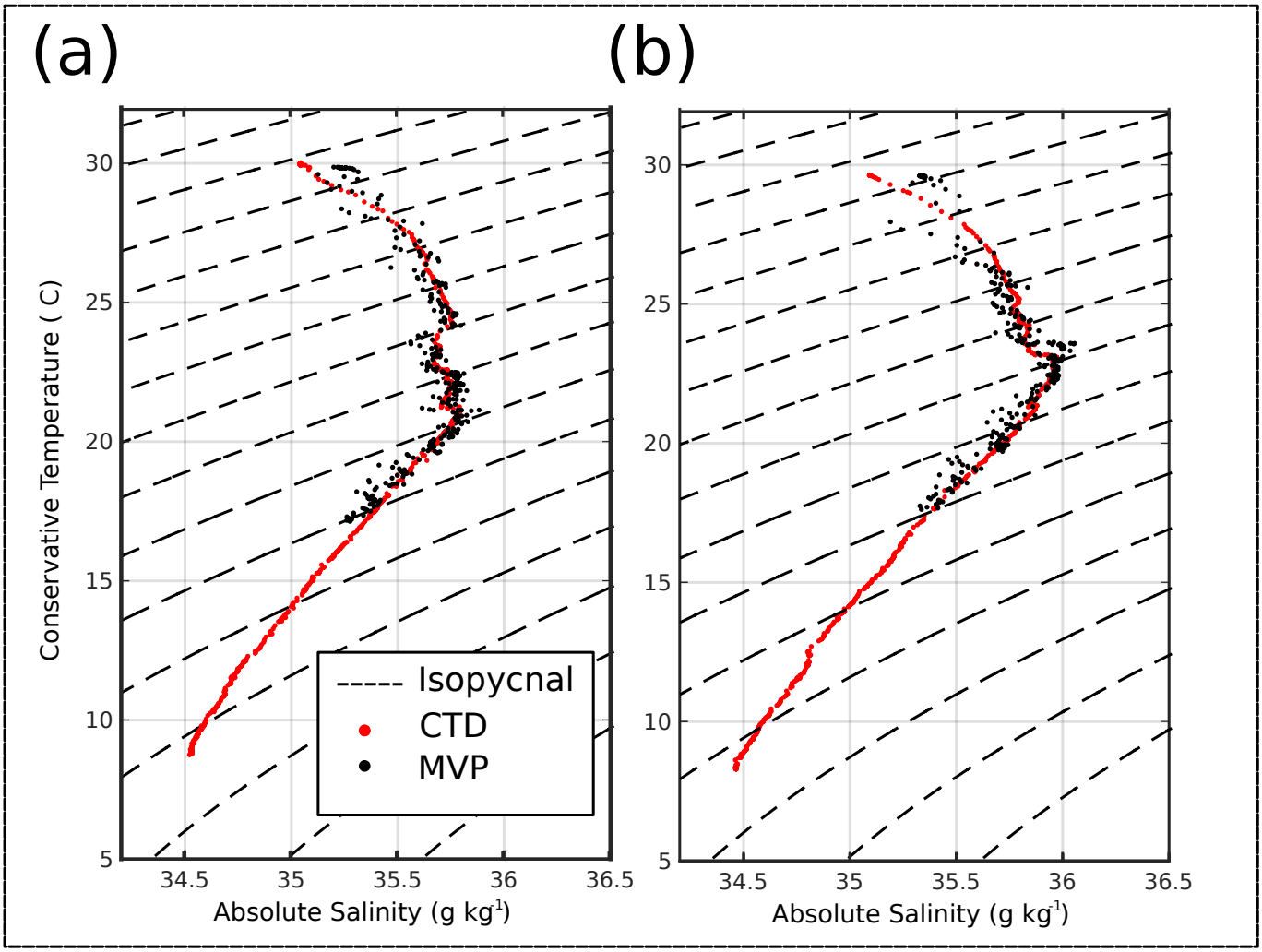

Figure 1: T-S diagram of two calibration casts between the MVP and CTD. (a) Cast outside of the transects in this article. (b) Cast at the end of MVP transect T4 and adjacent to station SD13.

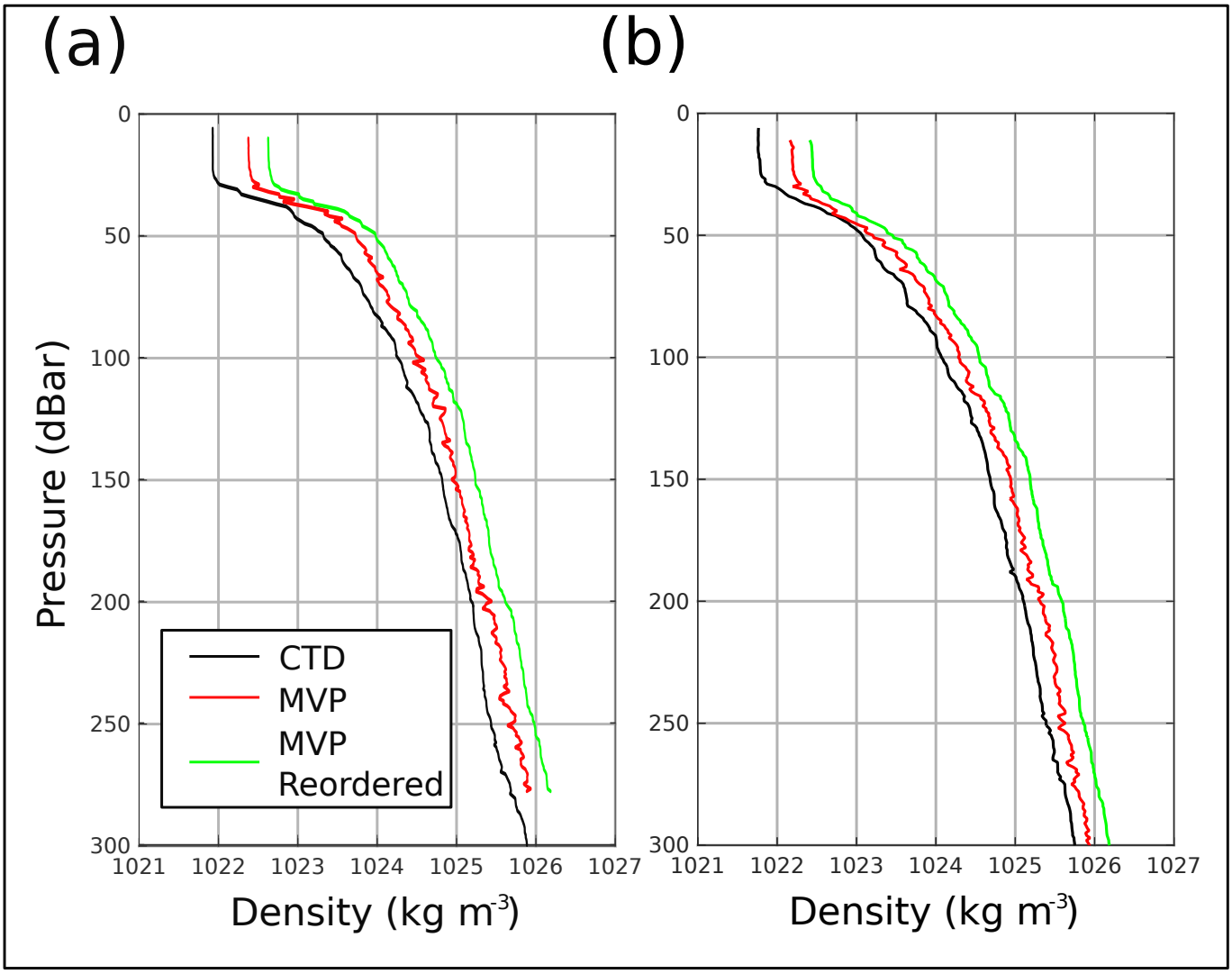

Figure 2: Resulting density profiles from two calibration casts in Fig. S1. Subsequent density profiles are offset from each other by 0.25 kgm^{-3}

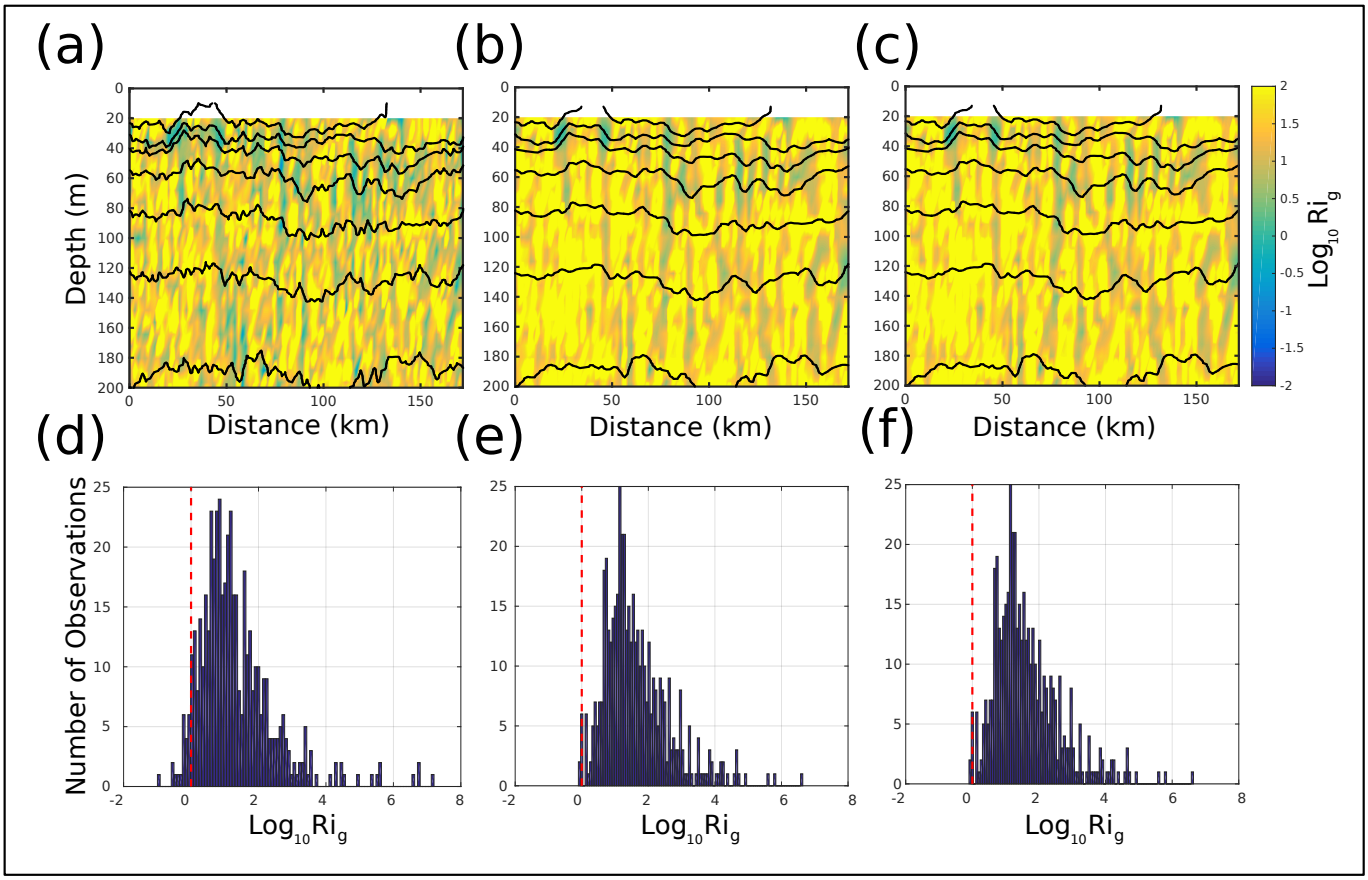

Figure 3: Effects of horizontal filtering of density on the Richardson number, starting with (a) unfiltered, (b) 9 km filtered, and (c) 32 km filtered data for transect T4. Shading and isopycnal values are the same as Fig. 5b. Histograms for the three treatments are shown in (d-f) underneath their respective filtering. Red dashed line depicts critical value of 1 for Ri_g.

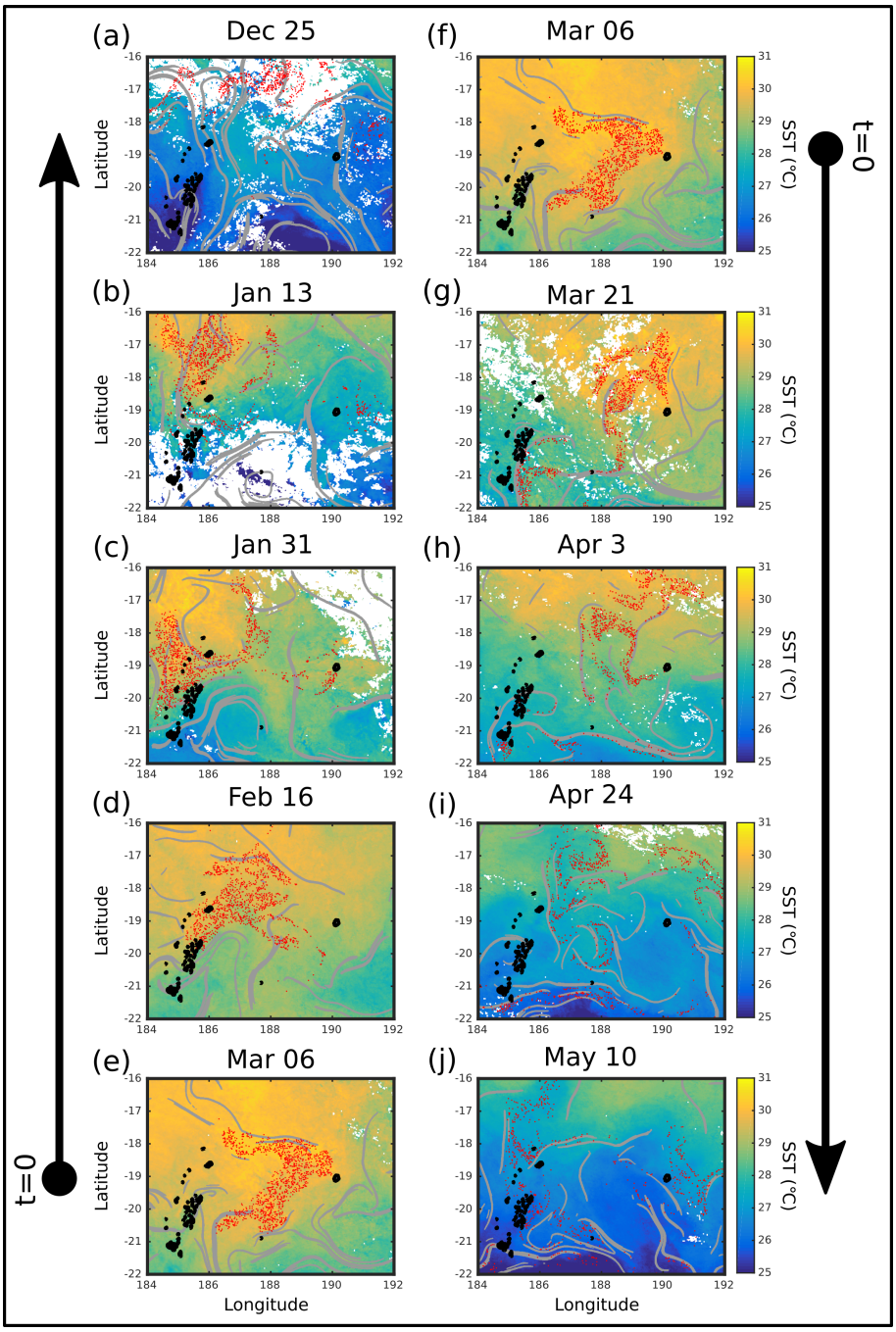

Figure 4: Same as Fig. 6, with SST values instead of chl-*a*.

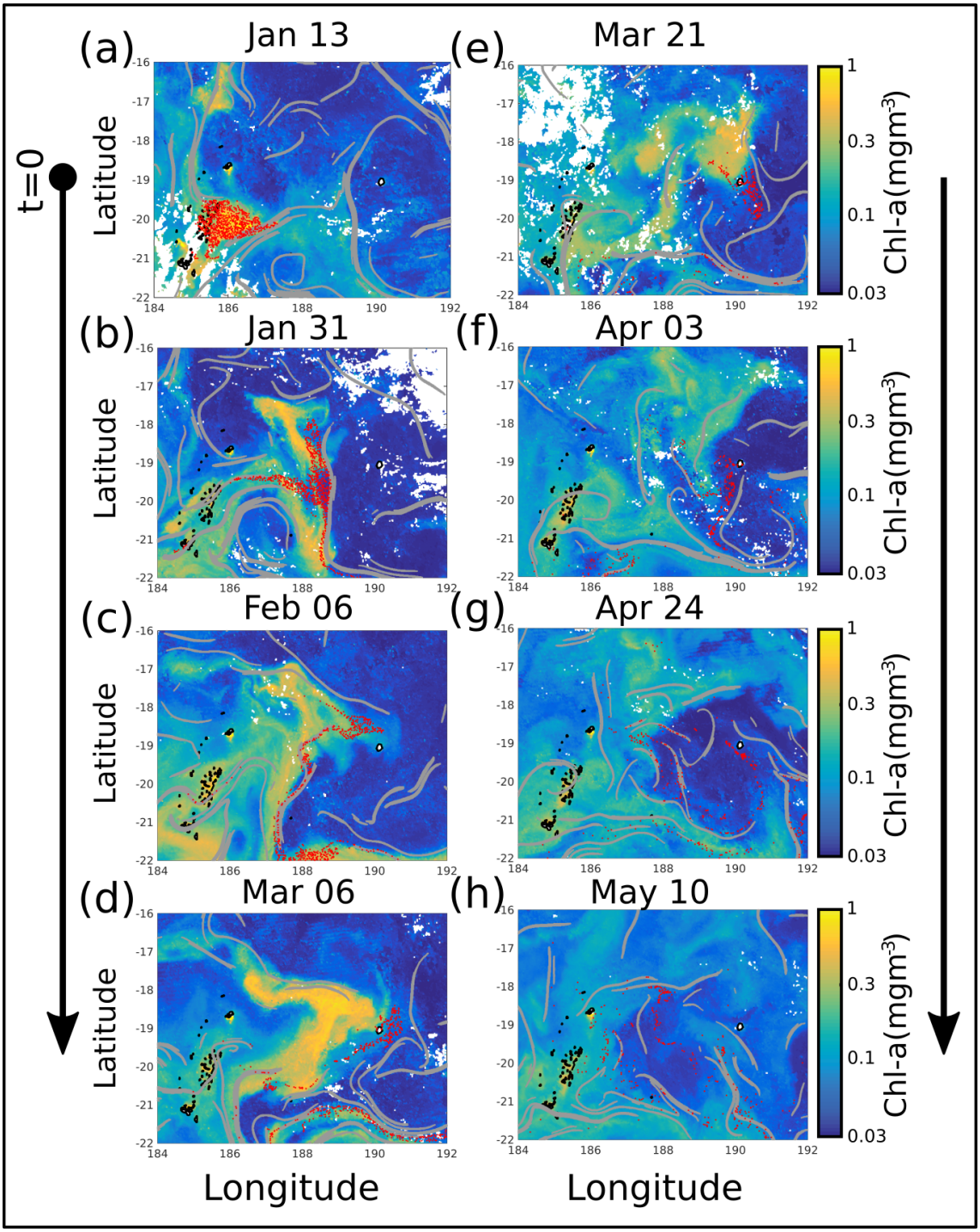

Figure 5: Similar to Fig. 6, but with ARIANE particles seeded on Jan 13 in a forward integration.

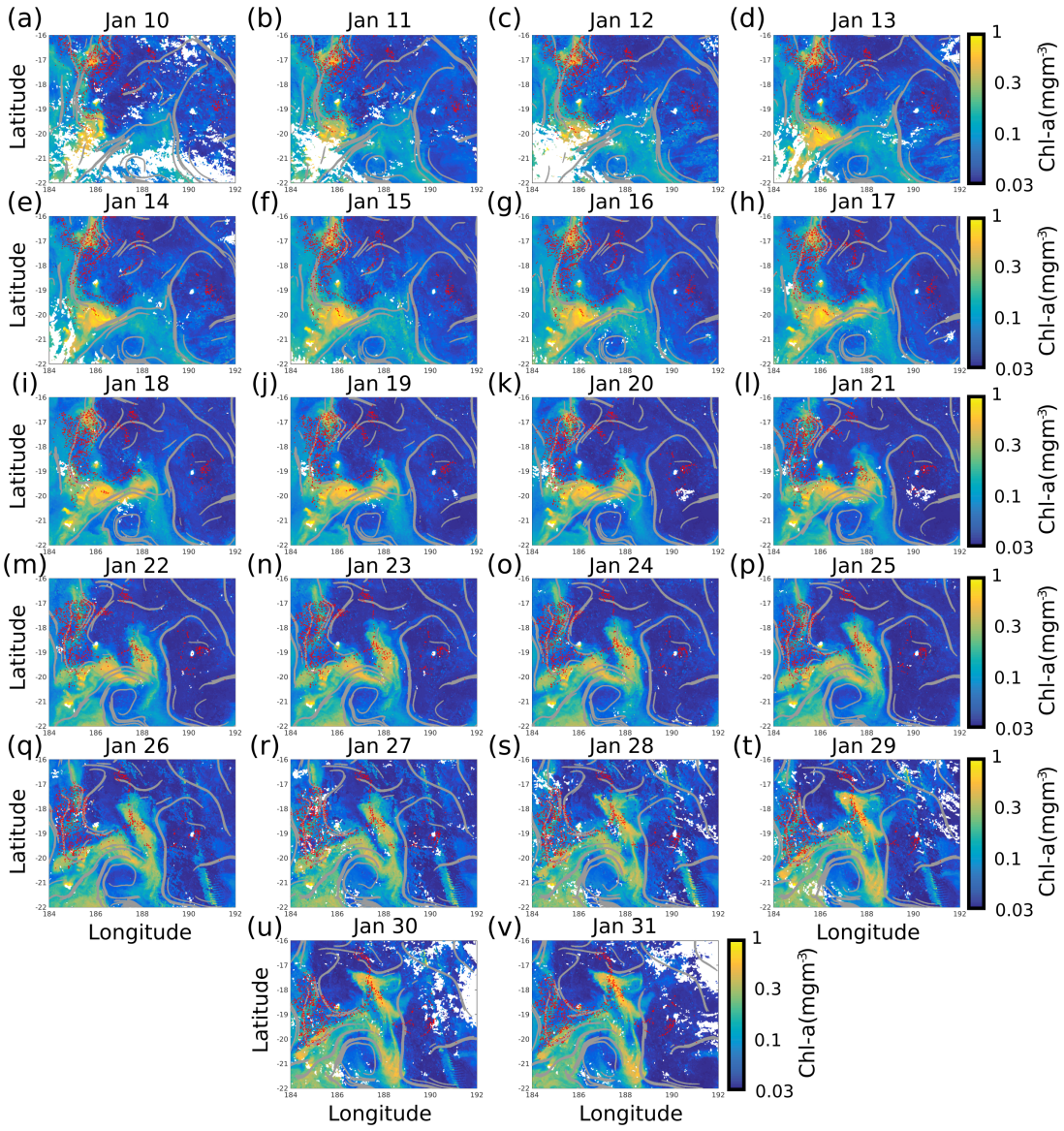

Figure 6: Similar to Fig. 6, but for additional dates ranging from Jan 10 to Jan 31.

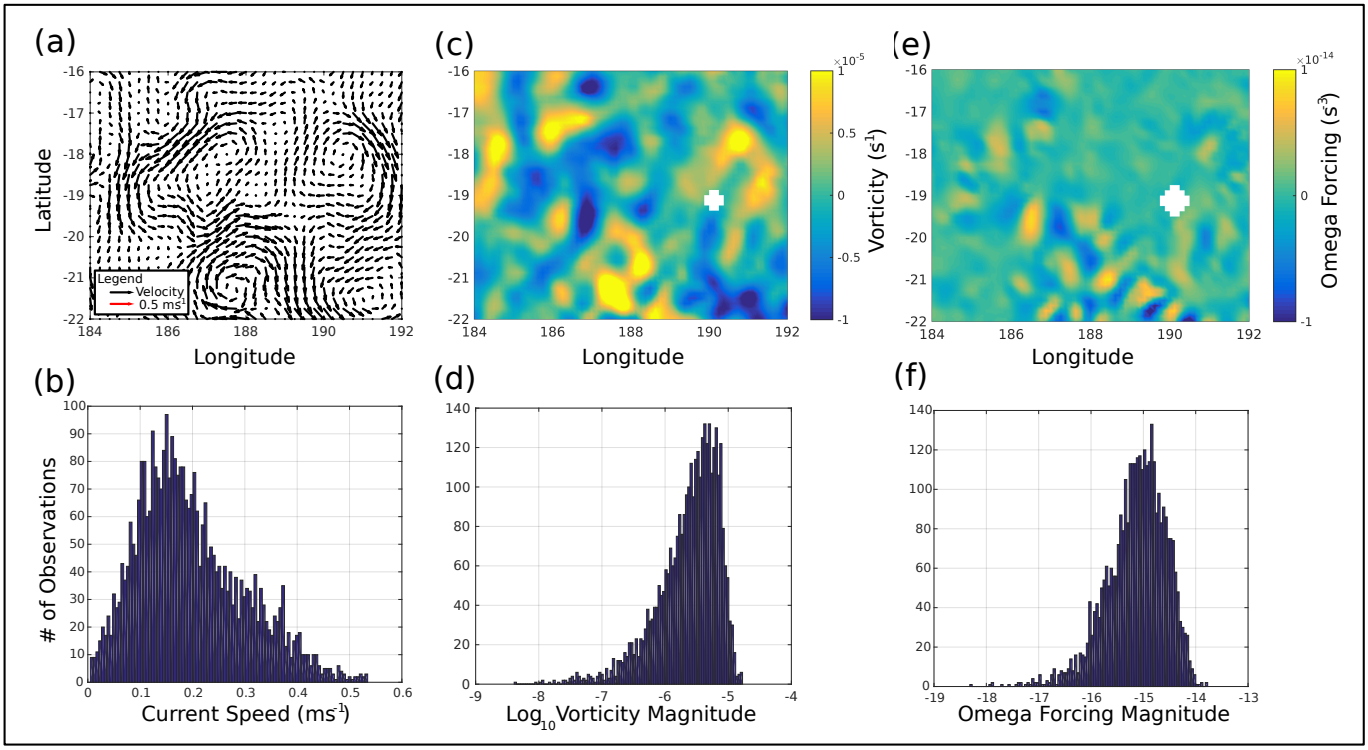

Figure 7: Impact of frontogenetic forcing on bloom initiation on Jan 13. (a) Velocity currents and (b) histogram of their magnitude. (c) Spatial distribution of relative vorticity and (d) histogram of its magnitude. (e) Spatial distribution of omega equation forcing term from Calil et al., (2011), along with a histogram of its magnitude.

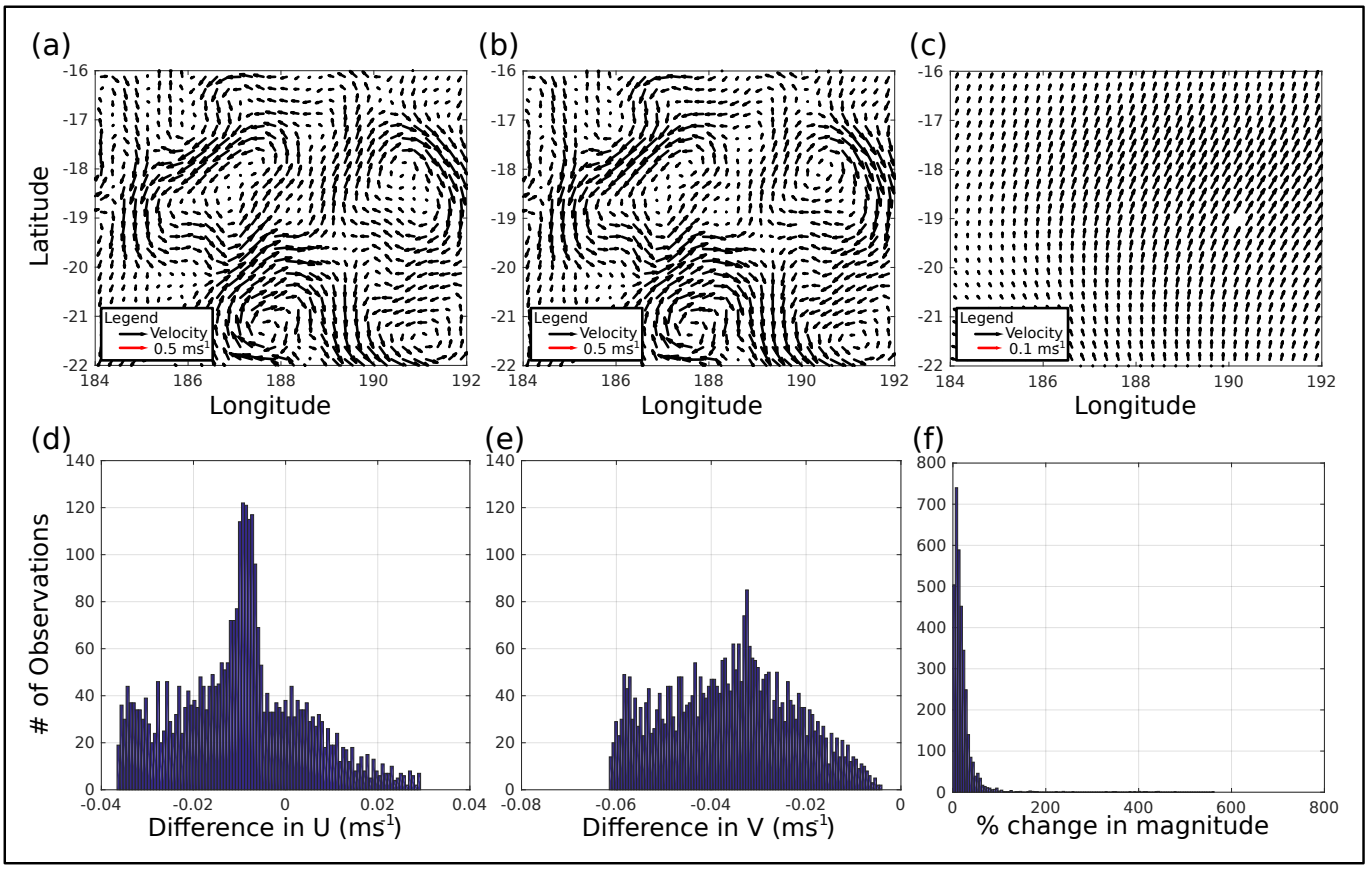

Figure 8: Comparison of CNES velocity products with and without Ekman wind effects. Spatial distribution of currents on Jan 13 (a) without and (b) with Ekman wind effects, along with (c) differences between the two. Histograms of the difference in (d) u, (e) v, and the (f) percent change in magnitude with the addition of wind.

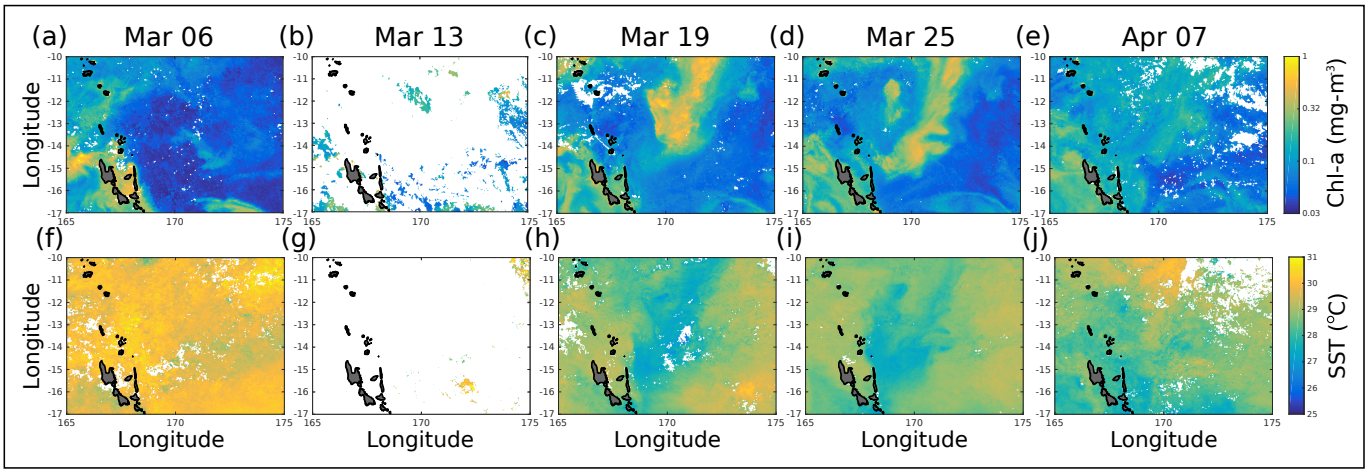

Figure 9: Timeseries of satellite surface (a-e) chl-a and (f-j) SST from early March to early April, 2015, before and after Cyclone Pam. The islands shaded in grey are part of Vanuatu.

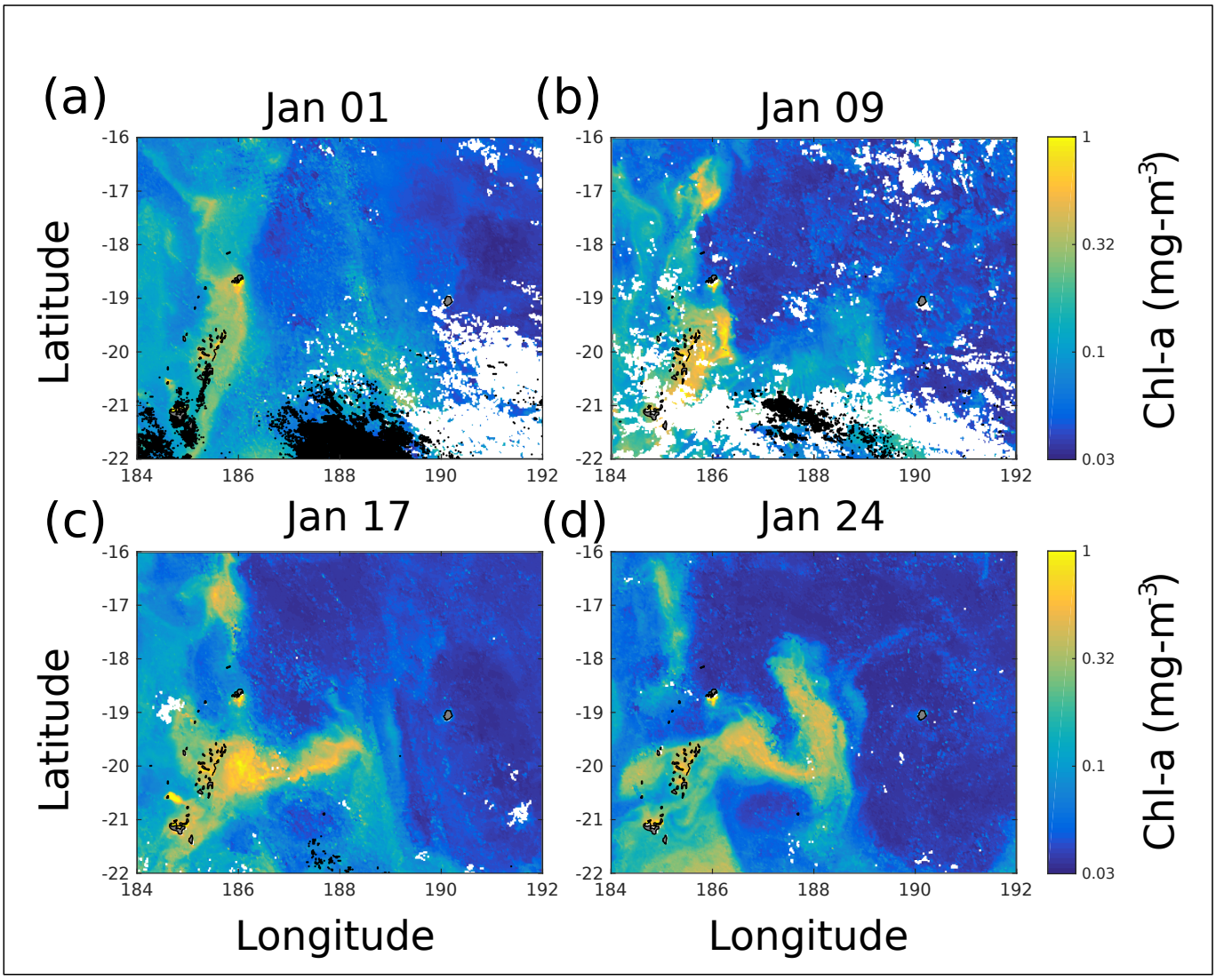

Figure 10: Timeseries of satellite surface chl-a for (a) Jan 1, (b) Jan 9, (c) Jan 17, and (d) Jan 24 for the LDB region. Pixels with SST values of 25 or below are shown in black.